

REPORT DOCUMENTATION PAGE

Public reporting burden for this collection of information is estimated to average 1 hour per response, including the time for reviewing instructions, maintaining the data needed, and completing and reviewing this collection of information. Send comments regarding this burden estimate or suggestions for reducing this burden to Department of Defense, Washington Headquarters Services, Directorate for Information Operations and Reports, Suite 1204, Arlington, VA 22202-4302. Respondents should be aware that notwithstanding any other provision of law, no person shall be subject to a collection of information if it does not display a currently valid OMB control number. **PLEASE DO NOT RETURN YOUR FORM TO THE ABOVE ADDRESS.**

1. REPORT DATE (DD-MM-YYYY) 11-12-2006		2. REPORT TYPE Final Technical Report		3. DATES COVERED (From - To) 01-06-2001 to 30-06-2006	
4. TITLE AND SUBTITLE Chalcopyrite and Orientation-Patterned Semiconductors for Mid-IR Sources: Modeling, Growth and Characterization				5a. CONTRACT NUMBER	
				5b. GRANT NUMBER F49620-01-1-0428	
				5c. PROGRAM ELEMENT NUMBER	
6. AUTHOR(S) M.M. Fejer, N. Giles, J. Ketterson, R. Pandey, P. Kuo, A. Lin, O. Levi, R. Route, K. Vodopyanov				5d. PROJECT NUMBER	
				5e. TASK NUMBER	
				5f. WORK UNIT NUMBER	
7. PERFORMING ORGANIZATION NAME(S) AND ADDRESS(ES) Edward L. Ginzton Laboratory Stanford University Stanford, CA 94305-4088				8. PERFORMING ORGANIZATION REPORT NUMBER SPO No. 24498	
9. SPONSORING / MONITORING AGENCY NAME(S) AND ADDRESS(ES) AFOSR/NE 801 North Randolph Street, Room 732 Arlington, VA 22203-1977 <i>Dr Howard Schlossberg</i>				10. SPONSOR/MONITOR'S ACRONYM(S)	
				11. SPONSOR/MONITOR'S REPORT NUMBER(S)	
12. DISTRIBUTION / AVAILABILITY STATEMENT Approved for public release; distribution unlimited.					
13. SUPPLEMENTARY NOTES The view, opinions and/or findings contained herein are those of the author(s) and should not be construed as necessarily representing the official policies or endorsements, either expressed or implied, of the Air Force Office of Scientific Research or the U.S. Government.					
14. ABSTRACT The goal of this MURI was to advance the technology in chalcopyrite and microstructured zincblende semiconductors, and to demonstrate devices based on them. The program involved modeling, synthesis, characterization, and device demonstration. Research was focused on, (1) nonlinear chalcopyrites and microstructured zincblende crystals for applications to mid-infrared coherent sources, and (2) magnetic chalcopyrites for future application to spintronic and magneto-optic devices. We sought to enable applications such as compact high-power mid-IR sources for ICRM, and frequency-agile sources suitable for local and remote sensing of chemical and biological species. Research involved: (a) growth and characterization of orientation-patterned GaAs (OP-GaAs), a novel microstructured material with precisely engineerable properties for a wide variety of mid-infrared devices, (b) demonstration of mid-IR sources based on these materials, and their use in applications such as trace-gas detection, (c) understanding and ameliorating the effects of point defects and dislocations on the properties of established nonlinear chalcopyrites such as ZnGeP ₂ , and enabling the use of extremely promising but previously impractical materials such as CdGeAs ₂ , (d) pushing beyond microstructured into nanostructured GaAs nonlinear devices, a more speculative approach offering orders-of-magnitude improvements in device performance. For the magnetic chalcopyrites, the goal was synthesis of bulk and thin-film ferromagnetic semiconductors with Curie points above room temperature, and characterization of their magnetic and transport properties.					
15. SUBJECT TERMS micro-structured nonlinear optical materials, quasi-phases-matched mid-IR coherent sources, chalcopyrites, orientation-patterned GaAs and GaP, magnetic materials, magnetic chalcopyrites, spintronics					
16. SECURITY CLASSIFICATION OF:			17. LIMITATION OF ABSTRACT	18. NUMBER OF PAGES 34	19a. NAME OF RESPONSIBLE PERSON Martin M. Fejer
a. REPORT	b. ABSTRACT	c. THIS PAGE			19b. TELEPHONE NUMBER (include area code) (650) 725-2160

Chalcopyrite and Orientation-Patterned Semiconductors for Mid-IR Sources: Modeling, Growth, and Characterization

MURI 2001 FINAL TECHNICAL REPORT
November 2006

MURI - AFOSR Grant No. F49620-01-1-0428 (1 June 2001 through 30 June 2006)

PRINCIPAL INVESTIGATOR: Professor Martin M. Fejer

LEAD INSTITUTION: Stanford University

AFOSR PROG. MANAGER: Dr. Howard Schlossberg, <howard.schlossberg@afosr.af.mil>, (703) 696-7549

PROGRAM OBJECTIVE: The scientific goal of this MURI effort was to advance the state-of-the-art in chalcopyrite and microstructured zincblende semiconductors, and to demonstrate devices based on these improved materials. The program was a vertically integrated effort involving modeling, synthesis, characterization, and device demonstration. The research was focused on two major classes of these materials, (1) nonlinear chalcopyrites and microstructured zincblende crystals for applications to mid-infrared coherent sources, and (2) magnetic chalcopyrites for future application to spintronic and magneto-optic devices. The nonlinear materials enabled applications such as compact high-power mid-IR sources for IRCM, and frequency-agile sources suitable for local and remote sensing of chemical and biological species. For the nonlinear materials, there were several major areas of research: (a) growth and characterization of orientation-patterned GaAs (OP-GaAs), a novel microstructured material with precisely engineerable properties for a wide variety of mid-infrared devices, (b) demonstration of mid-IR sources based on these materials, and their use in applications such as trace-gas detection, (c) understanding and ameliorating the effects of point defects and dislocations on the properties of established nonlinear chalcopyrites such as ZnGeP_2 , and enabling the use of extremely promising but previously impractical materials such as CdGeAs_2 , (d) pushing beyond microstructuring into nanostructured GaAs nonlinear devices, a more speculative approach offering orders-of-magnitude improvements in device performance. For the magnetic chalcopyrites, the goal was synthesis of bulk and thin-film ferromagnetic semiconductors with Curie points above room temperature, and characterization of their magnetic and transport properties.

MURI CONSORTIUM RESEARCH TEAM MEMBERS:

- **Stanford University:** Prof. Martin M. Fejer (P.I.), Prof. Robert L. Byer, Prof. Robert S. Feigelson, Prof. James S. Harris
- **Michigan Technical University:** Prof. Ravi Pandey
- **Northwestern University:** Prof. John Ketterson
- **West Virginia University:** Prof. Nancy Giles, Prof. Larry Halliburton

FINANCIAL EXECUTION:

3-YEAR BASE PERIOD – FY01:\$470,580; FY02:\$1,000,000; FY03:\$1,000,00; FY04:\$417,108

2-YEAR OPTION PERIOD - FY04:\$661,468; FY05:\$1,000,000; FY06: \$450,844

As of (31 May 2004) all of the Base Period funds including the first FY04 increment, amounting to a total of \$2,887,688 had been completely paid to Stanford University, the consortium lead institution, were fully expended and were “off the government’s books”.

As of (30 June, 2006) all of the Option Period funds including the second FY04 increment, amounting to a total of \$2,112,312, had been completely paid to Stanford University, the consortium lead institution, were fully expended and were “off the government’s books”.

SCIENTIFIC APPROACH: To achieve the above scientific objectives, the MURI participants and collaborators worked along the following synergistic lines: Stanford and collaborators at Hanscom AFB (David Bliss) focused on Objective #1a (section numbers refer to following paragraphs), with the former using MBE and photolithography to create orientation templates, and the latter growing thick films on these templates by hydride-vapor-phase epitaxy. Additionally, Stanford researchers worked on developing similar materials technology for GaP and on growing waveguide-quality, low-scatter-loss OP-GaAs. The mid-IR source development described in Objective #1b was

20061212244

carried out at Stanford and in collaboration with industrial partners at BAE and Northrop-Grumman under the AF CARMA-I program (demonstration of high-power mid-IR optical parametric oscillator (OPO) sources for IRCM applications), and with collaborators at Sandia National Lab (demonstration of narrow linewidth sources for trace-gas detection). Such collaborations are expected to accelerate future transitions of the MURI technologies from the laboratory into the field. Novel tunable and broadband mid-infrared sources have been under continuous development at Stanford based on OPOs and optical parametric generators (OPGs). The chalcopyrite material synthesis and characterization studies of Objective #1c were carried at West Virginia University (relationship of optical and electronic properties to defects present), in collaboration with Stanford (synthesis of bulk chalcopyrite crystals) and Michigan Technological University (first principles quantum mechanical modeling of defect states). This portion of the program was carried out in close collaboration with BAE Systems, the quality of whose ZnGeP₂ crystals, and the performance of the IRCM devices on which they are based, had already been affected positively. The photonic nanostructures of Objective #1d were fabricated at Stanford, taking advantage of the electron-beam-lithography tools available at the Stanford Nanofabrication Facility. The magnetic chalcopyrites of Objective 2 were grown and characterized at Northwestern University.

CONCLUSIONS AND RECOMMENDATIONS FOR FURTHER STUDIES:

Overall, this five year MURI program has been highly successful in developing new materials and/or new materials technologies for mid-IR devices. Approval of funding for the two option years enabled extension of the proof-of-principle mid-IR device demonstrations in Stanford's OP-GaAs to more sophisticated devices with functionalities enabled by the engineerable material, addressing high-power (multi-watt for IRCM), spectrally-agile (multi-micron tuning range for sensors) and ultrafast (single-cycle mid-IR pulses can be supported in suitable OP-GaAs) applications. Initial device demonstrations in the nascent nanostructured III-V nonlinear materials were successfully carried out. Orientation patterning of GaP (initial results for which had already been obtained) were pursued to obtain a material extending the revolutionary advantages of OP-GaAs to a wider bandgap material. Because of their potential applications in infrared counter-measures for defense purposes, there is a compelling reason to pursue further development in the growth technology for OP-GaAs and related materials.

Much about the nature of point defects in device-quality CdGeAs₂ (the most highly nonlinear phasematchable mid-IR crystal known) and mixed CdGeAs₂-CdGeP₂ crystals emerged from the WVU-Stanford-MTU collaboration. Further improvements in ZnGeP₂ performance are anticipated. Growth of magnetic chalcopyrites films on GaAs at NWU will enable studies of interface properties relevant to, e.g. spin injection for spintronics; collaboration between NWU and Stanford on growth of low-defect Mn-doped chalcopyrites essential for high-mobility ferroelectric semiconductors will be pursued.

HIGHLIGHTS:

1a) Orientation-patterned GaAs (OP-GaAs) and GaP (OP-GaP) – materials development and characterization

- Significant improvements in OP-GaAs template quality and hydride vapor phase epitaxy (HVPE) thick film growth were made. High quality, low surface roughness templates were grown reproducibly, while the subsequent HVPE growth for bulk samples achieved thicknesses up to 750μm in one step with high fidelity domain periods down to 40 microns.
- Loss characterizations of thick-film OP-GaAs showed improved uniformity across the sample and losses in recent samples as low as 0.005 cm⁻¹.
- Improved gallium arsenide dispersion relations allowed more accurate prediction of quasi-phasematching (QPM) conditions and the temperature dependence of QPM wavelengths.
- Demonstrations of domain inversion in the related zincblende material, gallium phosphide (GaP), using molecular beam epitaxy will enable growth of orientation-patterned GaP in future research programs.

1b) Development of Orientation-patterned AlGaAs waveguides

- The lowest loss to date for waveguides in orientation-patterned AlGaAs of ~4.5dB/cm at 1.55μm wavelength was demonstrated. The low loss is due to improvements in growth and processing and, in particular, by a reduction of the template height corrugation from ~130nm to 20nm.

- Fabrication of quasi-phases-matched AlGaAs waveguides for continuous-wave second harmonic generation (SHG) allowed record internal conversion efficiency of 23%/W. The waveguide was 5-mm long and was pumped at a wavelength near 1.55- μm .

1c) Orientation-patterned GaAs – device demonstrations

- The first pulsed, nanosecond-duration optical parametric oscillator (OPO), tunable over 2-11 μm , was demonstrated in OP-GaAs using a PPLN OPO pump in the 1.75-to 2.05- μm wavelength range
- The first demonstration of optical parametric generation (OPG) in OP-GaAs. The experiment produced an ultra-broadband mid-infrared continuum spanning 4.5 to 10.7 μm with 3.28- μm , 1-ps pump pulses up to 2- μJ energy. OPG was also used to study the interesting polarization dependence in OP-GaAs arising from its d_{14} nonlinear coefficient.
- Demonstration of a multi-grating, narrow-linewidth (sub-MHz) difference frequency generation source between 7.2 and 9.4 micron extending the capabilities for trace gas detection (in collaboration with Sandia National Laboratory under DOE support).

1d) Chalcopyrites for nonlinear optics - preparation, characterization and defect modeling

- Transition origins for three distinct photoinduced absorption bands in ZnGeP_2 were established; these bands cause pump-induced absorption, which limits laser device performance.
- Optical properties of substitutional copper acceptors in ZnGeP_2 were established; copper forms deep (0.62 eV acceptor level); neutral acceptor wavefunction established using EPR and ENDOR techniques.
- Optical properties of bulk CdGeAs_2 crystals were shown to be controlled by shallow donors and two discrete acceptor defects; these defects give rise to four discrete absorption bands that affect nonlinear optical device performance.
- Variations in the stoichiometry of CdGeAs_2 crystals were monitored by comparing the intensity of photoluminescence bands associated with shallow acceptors (possibly Ge_{As}) and deep acceptors (possibly V_{Cd}).
- Site occupancy and charge states of transition-metal ions have been determined in chalcopyrite crystals (Mn^{2+} ions in ZnGeP_2 , Mn^{2+} ions in CdGeAs_2 , Cr^{2+} and Cr^{4+} in CdGeAs_2 , and Ni^{+} in AgGaSe_2); no evidence for Mn^{4+} on Ge^{4+} sites in CdGeAs_2 was found.
- Significant reduction in concentration of shallow acceptor in CdGeAs_2 can be produced by doping on anion site with Se or Te.
- Significant reductions in concentration of deep acceptors in CdGeAs_2 can be produced by doping on the Cd site with indium.
- CdGeAs_2 crystals doped with iron impurities exhibit reduced absorption losses.
- Consistent radial and axial variations in the optical properties of as-grown CGA boules were identified for the first time. The highest optical transmission was found midway down the boule length.
- The role of dislocations and their effect on optical properties in CGA was also revealed for the first time. Depending on composition they can either improve or increase optical absorption.
- The major advance in our cadmium germanium diarsenide crystal growth effort was the discovery that growth in the $\langle 112 \rangle$ direction both minimizes dislocation formation and substantially improves optical transmission and optical uniformity. All future crystal growth efforts on this compound should employ this growth orientation.
- An embedded quantum cluster model based on density functional theory for CdGeAs_2 was developed. A clear and distinct difference in the nature of native (i.e. Ge_{As}) and impurity (i.e. C_{As} and Si_{As}) antisite defects was predicted. The shallow acceptor in CdGeAs_2 was found to have a delocalized ground state. Experimental data was unable to conclusively make the assignment, and the computational modeling provided the only successful approach to find a model for the EPR signal.

1e) Fabrication and characterization of AlGaAs submicron waveguides and cavities

- An improved version of our waveguide structure, based on artificial birefringence, was demonstrated. The conversion efficiency was $\sim 20000\text{ \%}/\text{W}/\text{cm}^2$ (highest reported to date). Waveguides were fabricated and characterized. The device external efficiency ($\sim 4\text{-}5\text{ \%}/\text{W}$) was limited only by loss at the second harmonic. The location of the phasematching peak is ultimately set only lithographically (determined by varying the waveguide width).
- A resonant cavity embedded in the waveguide and resonant at the fundamental wavelength, to further increase efficiency, was designed and fabricated. A novel "waveguide dichroic mirror" nanostructure was realized, reflecting at the fundamental and transmissive at the second harmonic.

1f) Application of orientation-patterned GaAs for generation of terahertz radiation

- With primarily DARPA support through FA9550-04-1-0465, up to 1 mW average power of THz radiation was generated with an optical-to-optical efficiency of 0.01%, and a frequency tunable from 0.65 – 3.4 THz in QPM GaAs. The THz radiation was generated using cavity-enhanced difference frequency generation using a picosecond, mode-locked pump source.

2) Experiments involving magnetic chalcopyrite and other semiconductors for potential Spintronic applications

- MnGeP₂: Extensive transport measurements were performed on MBE-grown thin films of MnGeP₂. The observation of a field-saturable anomalous Hall effect with accompanying hysteresis, along with direct magnetization measurements, confirmed that the material is ferromagnetic with a Curie temperature of 325K.
- MnAs: Epitaxial films of MnAs were deposited on silicon, gallium arsenide and germanium. Films on (100) GaAs can be prepared in a single-domain state and have strong in-plane magnetic anisotropy. It is suggested that this material has some potential as a memory element or as a source of spin-polarized electrons in GaAs.
- Cu:ZnO: Copper-doped zinc oxide thin films were shown to be ferromagnetic with a transition temperature above 350K.

TRAINING OF GRADUATE STUDENTS:

At the end of this 5-year MURI program, eight graduate students have completed Ph.D. dissertations.

PERSONNEL SUPPORTED:

Stanford

Faculty: 4
Staff: 3
Students: 13 supported
(5 Ph. Ds. Awarded)
Post-Docs: 3

Michigan Technological University

Faculty: 2
Staff:
Students: 1 supported
(1 Ph. D. awarded)
Post-Docs:

Northwestern University

Faculty: 1
Staff:
Students:
Post-Docs: 3

University of West Virginia

Faculty: 2
Staff:
Students: 3 supported
(1 Ph. D. awarded, 1 Ph.D. expected in 2006)
Post-Docs: 1

PAPERS PUBLISHED: 43

MAJOR ACCOMPLISHMENTS:

1a) Orientation-patterned GaAs and GaP for nonlinear optical applications

A key part of the project was the growth of thick-film OP-GaAs sample with various domain patterns for different device applications. The thick films (up to ~1-mm) were grown (by the group of Dr. David Bliss of Hanscom Air Force Base) by hydride-vapor-phase epitaxy (HVPE) on templates grown at Stanford by a combination of MBE and photolithography. Steady improvement in the growth of thick film OP-GaAs has occurred over the course of the program. Thicknesses over 1mm have been achieved in multi-step HVPE growths. Recently, OP-GaAs thick films with thicknesses up to 750- μm have been grown in a single step. The single-step growth runs avoid growth interruptions, which have been associated with excess loss at the boundary between two growths.

Recent thick films have also shown successful propagation of periods as small as 40 μm through 700- μm -thick films. Smaller periods have a tendency to "close-over" (terminate prematurely) due to the close proximity of domain walls. A slight imbalance between the growth rates of the two phases causes one of the orientations to overgrow the other, resulting in termination of the quasi-phases-matching grating. It was determined that the GaAs phase originating from the substrate of the template was more likely to overgrow the other phase and "dominate" the growth. By choosing the pattern of the template to have more areas of the less dominant phase, less overgrowth was observed and smaller periods grew to larger thicknesses before closing over. Figure 1 compares 40- μm -period OP-GaAs gratings grown in December 2005 to a recent growth. The domains in the earlier growth closed over before the end of the growth run, whereas in the recent growth, the domains propagate through the full 700- μm thickness.

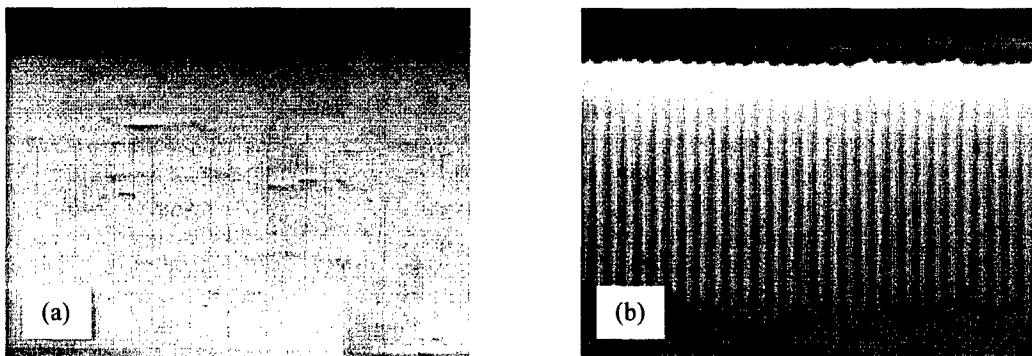


Figure 1. Stain-etched cross-sections of 40 μm period gratings grown in (a) December 2005 and (b) recently. Both growths are 700 μm thick (in a single step), but the more recent growth shows very high domain fidelity through the entire thickness whereas the earlier growth shows the domains terminating at about 460 μm thickness.

Losses in OP-GaAs thick films have been characterized with various laser sources. A measurement apparatus using a CW 2.015- μm -wavelength Ho:YAG non-planar ring oscillator (NPRO) laser was set up to characterize the loss. Scanning the sample showed that, until recently, the 2- μm loss in the OP-GaAs varied as a function of height in the samples. The loss tended to decrease towards the top of the sample, which corresponded to material grown later in the growth run. Recently grown samples measured with the same apparatus showed a much more uniform loss profile, which indicated improved control over time of the HVPE growth. These same measurements showed losses in the OP-GaAs of 0.005 cm^{-1} or lower, which is nearing the sensitivity limit of the measurement technique.

Orientation-patterning has allowed GaAs to become a practical nonlinear optical material, whose use required a more accurate dispersion model than that which existed prior to this program. Careful measurements of the GaAs dispersion and its temperature dependence were made by Skauli, et al. based on FTIR spectroscopy, Fabry-Perot reflectivity measurements, and second harmonic phasematching wavelengths. The dispersion was fit to a functional form, first proposed by Pikhtin, given by

$$n^2(\hbar\omega) = 1 + \frac{A}{\pi} \ln \left(\frac{E_1^2 - (\hbar\omega)^2}{E_0^2 - (\hbar\omega)^2} \right) + \frac{\langle \varepsilon_2 \rangle}{\pi} \ln \left(\frac{E_2^2 - (\hbar\omega)^2}{E_1^2 - (\hbar\omega)^2} \right) + \frac{G_3}{E_3^2 - (\hbar\omega)^2},$$

where the parameters E_0 , E_1 , E_2 , and E_3 were allowed to vary with temperature so that dn/dT and d^2n/dT^2 data could also be described. Tuning behavior predicted with these relations agree well with experimental data across the entire mid-IR range.

We have recently applied the orientation-patterning technology to the GaP/Si system. This system is particularly attractive because of the lower dispersion and greater transparency window for GaP compared to GaAs. We have developed recipes to grow single-phase GaP on Si for both orientations, thus providing a foundation for the growth of orientation-patterned GaP. Growth temperature has been identified as the most important parameter that determines which phase can be grown on vicinal Si substrates. We also found that the smoothest surfaces were achieved with a P_2 /Ga flux ratio as low as possible while still maintaining the growth in the P_2 -stabilized regime. Our study shows a P_2 /Ga flux ratio around $3\times$ is close to the optimum growth condition. Table 1 shows the GaP phases under different growth conditions. The OP-GaP template is grown based on the growth conditions obtained above. The growth condition #1 and #3 are used in the template growth. Si substrates with 4° off (001) towards [110] are used. Figure 2 shows the process flow of the OP-GaP template. First, single phase GaP (phase (111)A) ~ 30 -100 nm is grown on Si using the growth condition #3. Then, the GaP film is patterned and chemically etched to expose the alternate GaP and Si surfaces. A second single phase GaP (phase (111)B) is then grown on the exposed Si surface using the growth condition #1. At the same time, the GaP deposited on original GaP surface preserves the (111)A phase. Figure 3 shows a cross-sectional SEM image of the OP-GaP template regrown on this structure. An anisotropic chemical etch is utilized to reveal the domain boundaries. The image shows that two different orientations are preserved during the regrowth for a period as narrow as $4.8 \mu\text{m}$, although the domain boundaries between different orientations are not vertical. It is expected the regrowth of a template with a wider period ($>10 \mu\text{m}$ for bulk nonlinear generation) will have much better quality, good enough to provide a seed for further GaP growth by HVPE.

Table 1. GaP phases on Si under different conditions

Growth condition number	Nucleation Temperature ($^\circ\text{C}$)	Pre-layers	GaP Phases	Surface Roughness
1	350 $^\circ\text{C}$	P_2	(111)B	OK
2	350 $^\circ\text{C}$	Ga	(111)B	Worst
3	500 $^\circ\text{C}$	P_2	(111)A	Best
4	500 $^\circ\text{C}$	Ga	(111)B	OK

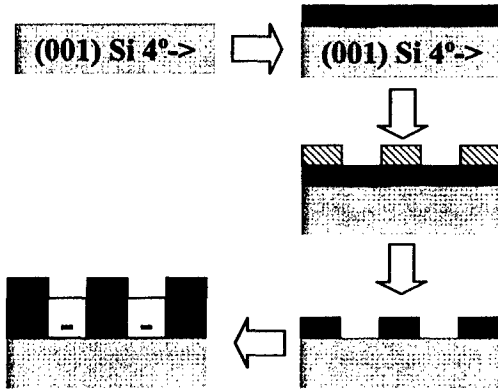


Figure 2. Process flow of OP-GaP template on Si substrates.

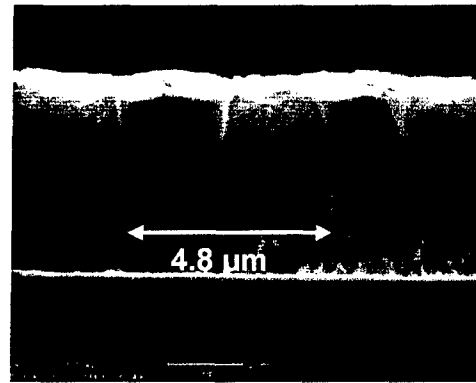


Figure 3. Cross-sectional SEM image of the OP-GaP template. Domain boundaries are revealed using anisotropic etching.

These experiments are on-track to achieve a multi-fold improvement in the conversion efficiency and power-handling capability of mid-IR NLO materials, which is a prime objective of the program.

Related Publications

1. D. F. Bliss and C. Lynch and D. Weyburne and K. O'Hearn and J. S. Bailey, Epitaxial growth of thick GaAs on orientation-patterned wafers for nonlinear optical applications, *J. Crystal Growth* **287**, 673-678 (2006).

1b) Development of Orientation-patterned AlGaAs waveguides

Over the two years, significant improvements have been achieved to improve the template quality, focusing on reducing the template corrugation and the domain-boundary corrugation, as well as improving the surface smoothness, which has important ramifications for low-loss waveguide structures. The inverted-GaAs/Ge/GaAs heterostructure growth conditions were also optimized to reduce the required layer thickness of GaAs on Ge to obtain single-phase epitaxy. Low offcut-angle substrates are now used, e.g., 1° rather than the conventional 4° , which has proven beneficial for the growth of GaAs on Ge. With this improvement and other necessary modifications of the growth conditions, GaAs with thicknesses of ~ 10 nm, compared to ~ 100 nm required in previous growths, were grown on Ge without the formation of antiphase defects. Thus, the template corrugation was reduced to ~ 20 nm from 130 nm, which helps obtaining better domain boundary quality during the re-growth. Figure 4 shows the cross-sectional TEM image of the low-corrugation film, which exhibits no defects at low template corrugations.

The fabrication of low-corrugation templates partially solves the issues of nonlinear waveguide devices fabricated on these templates. Previous nonlinear optical waveguides based on this approach were not as efficient as designed because the waveguide is very lossy. We found the loss in these earlier waveguides was induced by two different forms of corrugations, one is the template corrugation described above, but more importantly, the second is a corrugation formed during the waveguide regrowth, in which, deep grooves form at the domain boundaries. With our new template growth process, we are able to reduce the loss that is induced by the template corrugation. In order to reduce the second form of corrugations, the regrowth conditions of the nonlinear waveguides were investigated. We found that a low waveguide growth temperature suppresses the formation of these domain boundary grooves. Incorporating all these improvements, we were able to fabricate nonlinear waveguides with a loss of ~ 4.5 dB/cm at $1.55 \mu\text{m}$, the lowest ever achieved in microstructured AlGaAs waveguides. Figure 5 shows the SHG conversion efficiency for doubling a $1.55\text{-}\mu\text{m}$ cw-wave for the waveguides fabricated on two sets of samples, as testing platforms. The loss of samples #1869 and #1823 are 4.5 and 7.4 dB/cm, respectively. The optimum waveguide length to obtain the highest conversion efficiency is much larger when the waveguide loss is reduced.

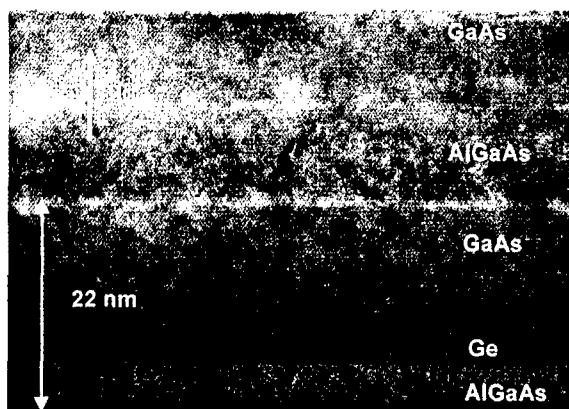


Figure 4. Cross-sectional TEM of the low-corrugation template.

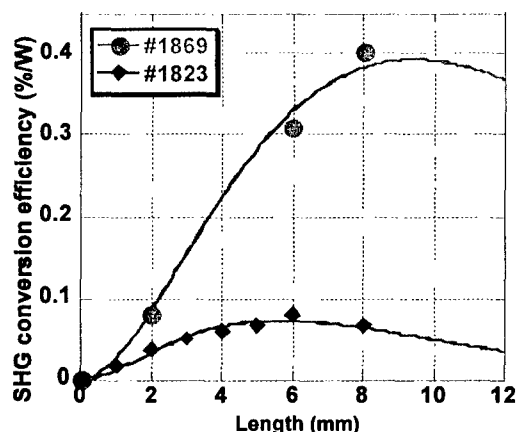


Figure 5. SHG conversion efficiency of the QPM waveguides with various lengths fabricated on various low-corrugation templates.

Figure 6(a) plots the SH output power vs the fundamental input power for a 5-mm-long and 5.8- μm -wide waveguide; the slope on the logarithmic plot is close to 2. This result indicates that the SH power has a quadratic dependence on the input power as expected for undepleted pump SHG. Figure 6(b) shows a typical second-harmonic tuning curve recorded with 4.25-mW input fundamental power (the power in front of the waveguide input facet), for a waveguide with a core of 1.1- μm $\text{Al}_{0.63}\text{Ga}_{0.37}\text{As}$ and cladding of $\text{Al}_{0.66}\text{Ga}_{0.34}\text{As}$, and a QPM period equal to 4.7 μm . The SH generation peaks at 1559.1 nm with the peak-power value at $\sim 0.61 \mu\text{W}$ after removing the Fabry-Perot enhancement effect. From figure 6, the external SHG conversion efficiency is estimated to be $\sim 3.4 \text{ \%W}^{-1}$. After taking into account coupling losses, Fresnel losses and the overlap efficiency, we obtained 0.85- μW internal-SH output with 1.91-mW internal-fundamental input, which corresponds to a normalized internal conversion efficiency of 23 \%W^{-1} , which is the highest ever reported for doubling 1.55 μm under CW operation in AlGaAs waveguides. This value is close to theoretical expectations after accounting for waveguide loss and QPM duty-cycle error.

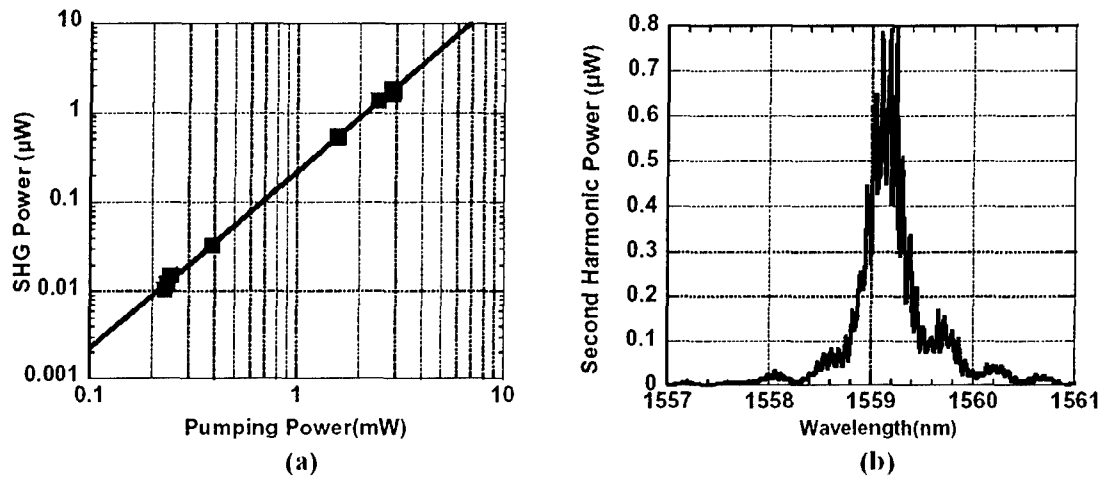


Figure 6. (a) Logarithmic plot of SHG output power versus fundamental input power in a 5-mm long AlGaAs QPM waveguide. (b) SHG output power as a function of the fundamental wavelength. Fringes are due to Fabry-Perot resonances at the pump wavelength.

Further improvements in QPM AlGaAs waveguides are expected, which will lead to higher conversion efficiencies and practical application of the waveguides for efficient mid-IR generation.

1c) Orientation-patterned GaAs – device demonstrations

Mid-Infrared Difference Frequency Generation (DFG) in OP-GaAs

During this program, we demonstrated a difference frequency generation (DFG) source coupled with either a multi-pass cell or a Cavity Ring Down Spectroscopy (CRDS) system, for gas phase analysis of trace gases. We improved the CRDS system to improve sensitivity, and included trigger circuits to exclude low amplitude ring-down signals.

Recently, we used a multi-grating OP-GaAs sample for wide tuning range, narrow linewidth DFG source. An OP-GaAs multi-grating crystal was grown using a combination of molecular beam epitaxy (MBE) and hydride vapor phase epitaxy (HVPE). The OP-GaAs sample had QPM periods of 23.8, 25.7, 26.7, 29.7 μm . An image of the 4-grating OP-GaAs structure is shown in figure 7a. Figure 7b shows continuous tuning of the idler wavelength for each one of the gratings in the multi-grating crystal, obtained by continuously tuning the pump and signal wavelengths at room temperature. Temperature tuning of the present four-QPM-grating crystal, or growth of a crystal with six QPM gratings, could fill the gaps in the spectrum. As a result, the whole spectral range between 7.2 and 9.4 μm can be scanned, thereby achieving a widely tunable, narrow linewidth source for mid-IR spectroscopy. This work was done in collaboration with Sandia National Laboratory (Livermore, CA).

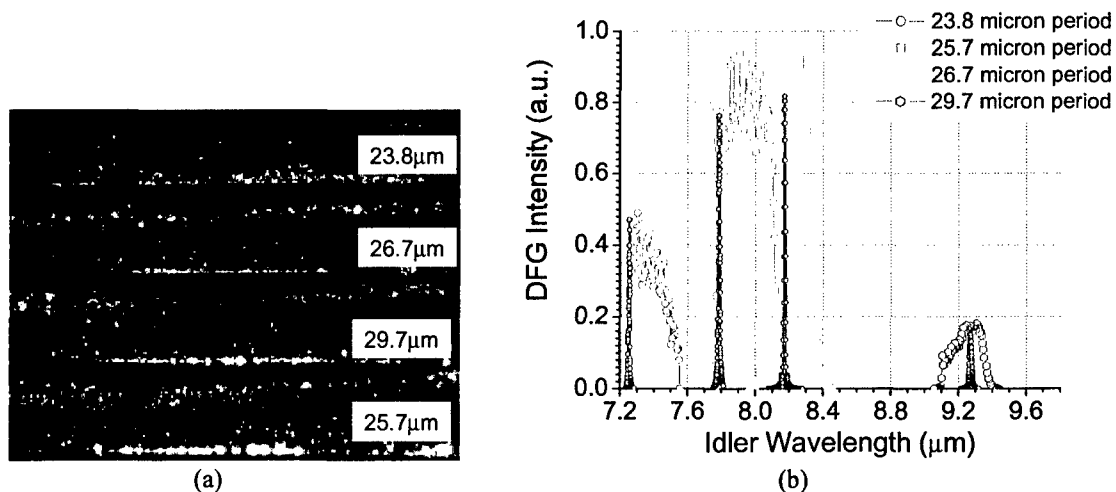


Figure 7. (a) Photograph of 4-period, OP-GaAs multigrating device. (b) DFG idler wavelength tuning in OP-GaAs for several QPM periods achieved by synchronously tuning pump and signal wavelengths. For comparison, the narrow curves show the idler when only one pump is tuned. Continuous tuning over this range would be possible in a suitable multi-grating sample.

OP-GaAs Optical Parametric Oscillator (OPO) Pumped with Nanosecond-duration Source

An OP-GaAs OPO was pumped with 1.75-to 2.05- μm wavelength, 6-ns pulses from a PPLN OPO that was in turn pumped with a Q-switched Nd:YAG laser (figure 8). By tuning the pump wavelength, the OP-GaAs OPO yielded continuous output from 2.07 to 3.08 μm (signal) and 5.8 to 11 μm (idler), as seen in figure 9. The pump threshold of the singly-resonant OPO was 16 μJ , which was consistent with theory, and the photon conversion slope efficiency reached 54%. The output wavelengths were only limited by the OPO mirror reflectivities, so with proper mirrors, tuning from 2 – 11 μm is possible.

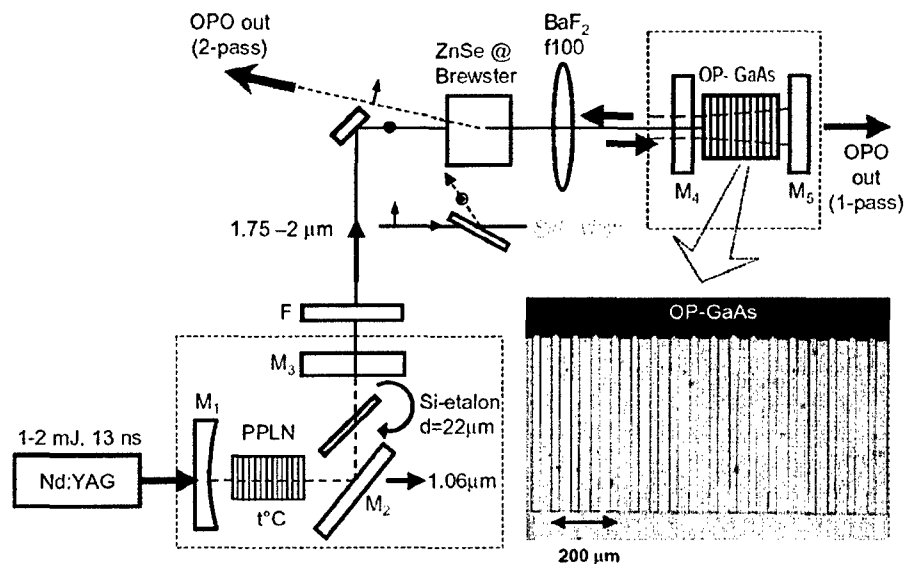


Figure 8. Schematic diagram of the OP-GaAs OPO. The inset shows a stain-etched cross-section of the 61.2 μm period OP-GaAs grating.

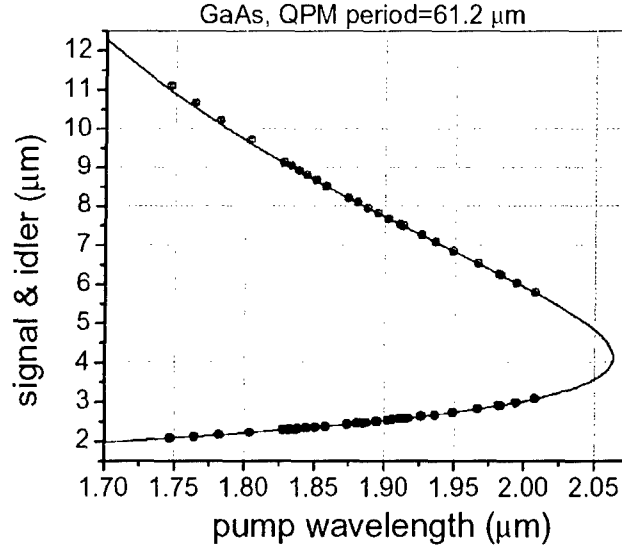


Figure 9. Measured OP-GaAs OPO tuning curve with respect to the pump wavelength (solid circles). Theoretical tuning is calculated from dispersion relation in Skauli [2003].

Optical Parametric Generation (OPG) in OP-GaAs

We recently demonstrated optical parametric generation (OPG) in OP-GaAs that resulted in an ultra-broad mid-infrared output spectrum spanning 4.5 to 10.7 μm , measured 20 dB down from the peak. We pumped a 166.6-mm period OP-GaAs grating with 3.28- μm wavelength, 1-ps duration pulses with energy up to 2 μJ and observed a spectrum more than an octave wide. Such anomalously wide tuning bandwidths for parametric processes are associated with the wavelength where the group velocity dispersion (GVD), $d^2k/d\omega^2$, goes to zero. The gain bandwidth can be increased further by parametric gain broadening. At high gain, the shape of the gain spectrum is determined more by the gain coefficient rather than the phase-mismatch, illustrated in figure 10.

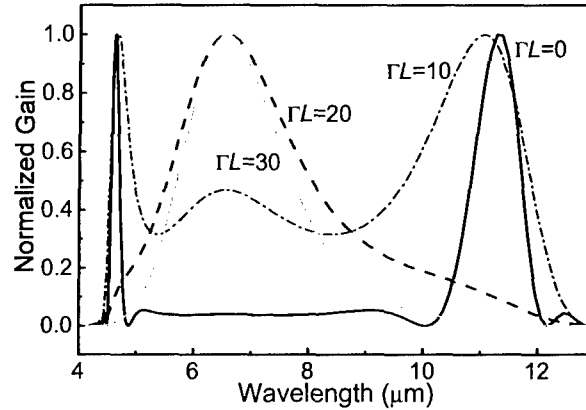


Figure 10. Theoretical gain spectra for 3.28- μm -pumped, 166.6- μm -period OP-GaAs sample for different values of ΓL (parametric gain coefficient). At small ΓL , the spectrum is peaked at the edges whereas at large ΓL , the spectrum is peaked at degeneracy.

Figure 11 shows the energy curve and the measured OPG spectrum. OPG threshold was observed at 55 nJ of pump energy. The observed spectrum was broad and peaked at degeneracy, which is expected from the parametric broadening due to the high pump intensities. The spectrum is actually broader than the detection range for our MCT detector, which is limited to $\lambda < 11 \mu\text{m}$. Dips in the spectrum, marked a and b in the figure, are due to parasitic sum frequency generation ($3.28 \mu\text{m} + 5 \mu\text{m} \rightarrow 1.98 \mu\text{m}$) that depletes the OPG spectrum at $5 \mu\text{m}$ and also lowers the gain at the corresponding idler at $9.5 \mu\text{m}$.

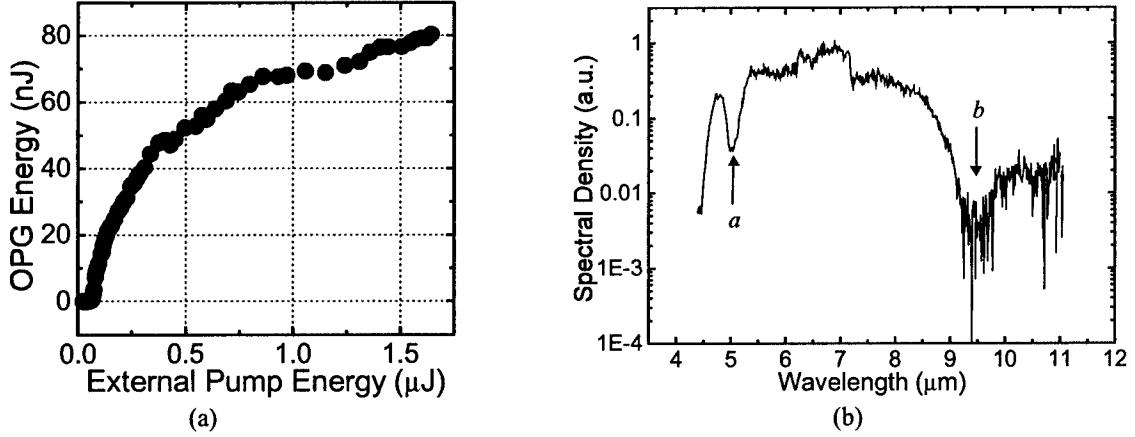


Figure 11. (a) Total OPG energy as a function of incident pump energy. Threshold was observed at 55 nJ. (b) OPG output spectrum for $3.28 \mu\text{m}$ pump at an energy of $1.4 \mu\text{J}$. Dips at 5 and $9.5 \mu\text{m}$ (marked a and b, respectively) are due to parasitic SFG.

Optical parametric generation in OP-GaAs was also used to explore the interesting polarization behavior in GaAs that arises from its high symmetry. In OP-GaAs experiments, the waves typically propagate along the $[1\bar{1}0]$ crystal direction. When all three polarizations are aligned parallel to $[111]$, the effective nonlinear coefficient, d_{eff} , is maximized with a value of $2d_{14}/\sqrt{3}$. When one of the waves is polarized along the $[110]$ direction (for definiteness, say it is the pump), it can be shown that $d_{\text{eff}} = d_{14}$, constant for all signal polarizations so long as the idler wave is complementarily polarized. As a result, OP-GaAs can be used in polarization-insensitive optical parametric amplification or in an optical parametric oscillator that is pumped with an unpolarized laser.

We studied the OPG dependence on input pump polarization and compared the results to theoretical expectations. In figure 12a, we calculate d_{eff} as a function of pump polarization for the OPG or OPO process. We observe that d_{eff} varies from a minimum of d_{14} up to $2/\sqrt{3} d_{14}$, which implies that all pump polarizations can be efficiently utilized by OP-GaAs. Circularly polarized or even an unpolarized pump can be used with OP-GaAs. In contrast for periodically poled LiNbO₃, a pump polarized along $[001]$ is significantly more efficient for OPG or OPO than any other incident pump polarization. The observed OPG as a function of incident pump polarization is plotted in figure 12b. We see good qualitative agreement between the experiment and the calculated dependence of OPG on pump angle (noting that unsaturated OPG is an exponential function of d_{eff}). Maxima were observed at 35° , 145° , etc. when the pump is parallel to $\langle 111 \rangle$ crystal directions. Both the theory and the experiment showed differences in the shape of the minima at 0° ($[110]$) as compared to at 90° ($[001]$).

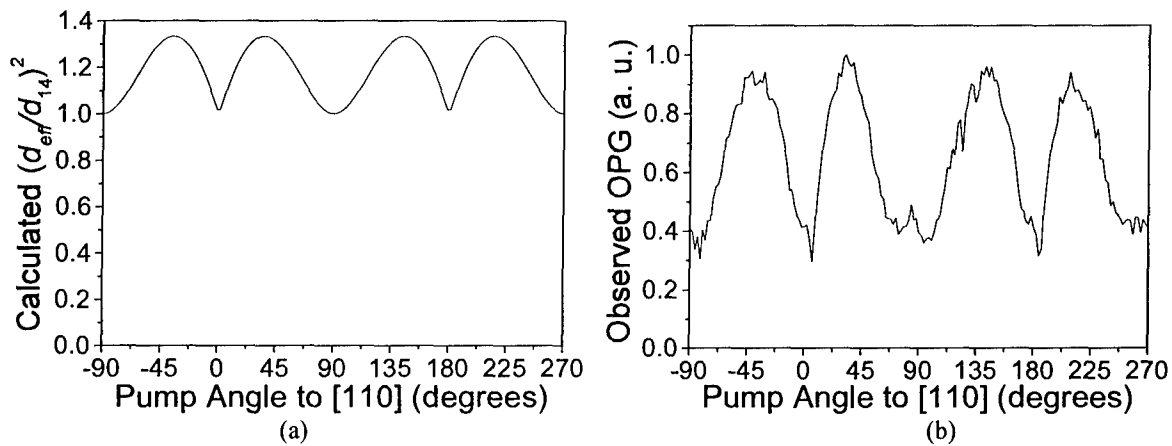


Figure 12. (a) Effective nonlinear coefficient for OPG for different pump polarization angles; (b) observed OP-GaAs optical parametric generation as a function of pump angle to [110].

1d) Chalcopyrites for nonlinear optics - preparation, characterization and defect modeling

CdGeAs₂ Growth Studies:

Boules of CdGeAs₂ were grown at Stanford University by the horizontal gradient-freeze technique. A transparent furnace allowed observation of the solid-liquid interface during growth. Low-temperature gradients (0.5-2.0°C/cm) minimized the vapor transport of volatile components and a pyrolytic boron-nitride-coated graphite boat minimized “sticking” problems. The growth rate was approximately 1 mm/hr, and the growth temperature was approximately 662°C. These growth efforts were highly successful and resulted in a set of samples suitable for characterization studies, both at Stanford and at West Virginia University. Undoped crystals showed the typical absorption band at 5.3 microns that is assigned to intravalence band transitions. The Stanford-grown material was comparable in quality to undoped p-type CdGeAs₂ crystals grown at BAE Systems.

Correlations Between Etch Pit Density and Absorption for [001] and [112] Growth Directions:

Cross sectional plates perpendicular to the growth direction [001] were cut from a number of single crystal boules of CGA, including those grown with 1% excess cadmium, germanium, or arsenic. These plates were polished and then etched in a mixture of nitric and hydrofluoric acids and water (1:1:2). Microscopic examination revealed the presence of etch pits associated with dislocations. The etch pit density (EPD) was nonuniform, being higher at the edges than in the center of the crystal. An infrared imaging system (2 to 5 μm range) showed that these plates were more transparent in the regions of high EPD. Similar results were obtained for the crystals that were grown with excess Cd, Ge, or As. Growth with excess As produced material with lower overall EPD and uniform high absorption in the 2 to 5 μm range, i.e., the region near the band edge. These crystals, however, had much lower intervalence-band absorption at 5.5 μm.

Nomarski optical microscopy revealed a pattern of striations on cross-section slices. Sets of three orthogonally oriented plates were cut from several of the crystals, polished, etched, and examined by Nomarski microscopy. Analysis of the striation patterns showed that they were associated with a pair of crystallographically related planes – (112) and (-1-12). These planes are the growth interface for CGA crystals growing in the [001] direction and are also the slip planes responsible for the dislocations observed in the initial etching studies. Based on these results, several crystals were then grown in the [112] direction. These crystals were cut, polished, and etched as before. Under microscopic examination, the cross-sections showed low EPD except for regions very close to the edges in some cases. Infrared imaging revealed that the transparency region coincided with the region of low EPD, which was a large fraction of the crystal. Nomarski studies showed that the growth interface consisted of three crystallographic planes, (102) and (012) on the sides and (11-2) on the bottom. Based on these results, subsequent crystals were grown along the [112] direction. Samples cut from [112]-growth direction boules were similar to the best CdGeAs₂ provided by BAE for our studies.

Axial Distributions of Optically Active Defects:

The intervalence-band optical absorption at 5.5 μm has been found to depend on position along the growth axis of a boule. It is lowest near the center and increases at each end, which suggests that more than one species (native defect and/or impurity) is responsible for the optical behavior. One species is more readily incorporated at the beginning of crystallization (distribution constant $k > 1$) and one is less easily incorporated ($k < 1$).

Growth of Doped CdGeAs₂:

One approach to improving the optical transparency of CGA is to incorporate dopants into the crystal to compensate the active species. To this end, eight [112]-oriented CGA crystals were grown with different dopants at varying concentrations. Two of the crystals incorporated selenium at 20 and 1000 ppm. A third crystal was grown which incorporated selenium at 1000 ppm, replacing an equivalent amount of As. Two were grown with chromium (100 and 1600 ppm), two with indium (10 and 100 ppm), and one with tellurium (500 ppm). The best results in terms of low optical absorption at 5.5 μm were obtained with 10 ppm of In. Boules were also grown that were separately doped with 1000 ppm of Mn, 1000 ppm Fe, and 1000 ppm Cu. The Mn-doped boule was oriented by x-ray Laue and cut into research-sized samples for characterization at WVU.

Growth of CdGe(As_{1-x}P_x)₂ Crystals

The goal of the CGAP studies is to engineer the band gap of the material to produce more efficient nonlinear devices. The optimal composition seems to be CdGe(As_{0.6}P_{0.4})₂. Because of the difference in melting points of CGA and CGP, the melting temperature of the intermediate solid solution increases approximately 1.3 °C per atomic % phosphorous. The difficulty lies in obtaining seeds of a composition that will not melt but will still be “wetable” as we move to higher phosphorous content. The current approach is to move up in P content in small increments and use the first part of a previous boule, which has a higher P content since $k > 1$ for P, as a seed for the next growth. Microprobe analysis was performed on the unseeded boule to determine the distribution of P along the boule length. The results are shown in the figure below. The phosphorus content is quite uniform in the center region, as expected from zone melting.

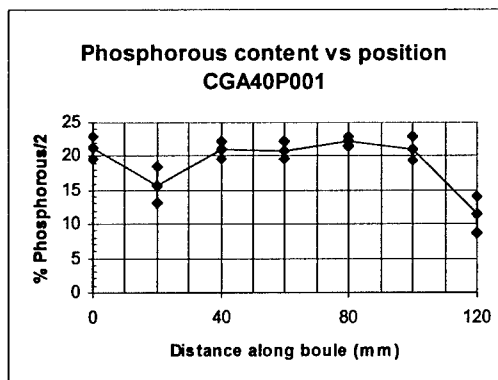


Figure 13. Variation of phosphorus along the length of a CdGeAsP boule, as determined by microprobe analysis.

Modeling of Defects:

Work at Michigan Technological University focused on the theoretical investigation of the electronic and structural properties of optically active defects in ZnGeP₂ and CdGeAs₂. To simulate the defects, a cluster-in-the-lattice technique was used, based on the *Gaussian 98* quantum mechanical code, and implementing a supercell technique within the *Crystal 98* code. The basis sets appropriate for bulk ZnGeP₂ were optimized using perfect crystal calculations, and these were then used in simulating defect clusters embedded in this material. To simulate the electrostatic embedding potential, atomic charges consistent with the perfect crystal ones are used to minimize the mismatch between the cluster and the surrounding lattice. In addition, a quantum embedding potential was

developed, which accounts for the short-range interaction with the lattice and confines the cluster wavefunction. This prevents the leaking of charge towards the lattice. Finally, the quality of this model was tested by means of self-embedding calculations, where the cluster represents a portion of the perfect lattice. When using a cluster model (with 270 point charges representing the electrostatic potential, 24 atoms described as quantum potentials, and 17 atoms on the quantum-mechanical cluster) to represent the pure crystal environment of a Zn atom in ZnGeP_2 , the nearest neighbor distances relax by less than 0.5% and the next-nearest neighbor distances relax by some 2%. This is a remarkably good agreement with the perfect lattice structure, and supports the accuracy of the model for use in simulating the electronic structure of point defects.

Full-scale calculations of paramagnetic defects V_{Zn}^- , V_{P} , S_{P} , and Se_{P} were performed using small clusters. We achieved a well-behaved model for the Zn vacancy (neutral and ionized), both electronically and geometrically. Modeling demonstrated that the unpaired electron in V_{Zn}^- is primarily localized on the first-neighbor P atoms. The negative vacancy formation energy, estimated to be 12.67 eV using an approximate model, is now calculated to be 5.93 eV, while that of the neutral vacancy is 1.42 eV. The latter shows a substantial localization of the extra electron within the empty site. Development of a corresponding model for the much more demanding anion (i.e. phosphorus-site) defect centers was undertaken. These donor centers show a much lower symmetry and lack an inversion center. For example, lack of inversion allows for the displacement of the P atom (in the self-embedding electronic structure calculations) or an impurity atom replacing the phosphorus (sulphur or selenium are being considered at this time) to displace from the perfect lattice position, whenever the embedding electric field is not perfectly balanced. This requires the addition of a further shell of neighboring atoms in the quantum mechanical calculation, for a total of 41 atoms, as compared with the 17 atoms of the Zn-site defect centers. In the case of the S and Se donors substituting for a P atom, the an interesting result is that the unpaired electron is mainly localized over the two Ge first-neighbors (40% each) and the impurity center (20%) but not over the two Zn first neighbors.

Defect Modeling of Group IV Antisites in CdGeAs_2 :

A theoretical study of the native and impurity group-IV antisite acceptor defects in CGA was performed. The calculated geometric relaxations and spin densities of the antisite defects considered here show a clear and distinct difference in the nature of native (i.e., Ge_{As}) and impurity (i.e., C_{As} and Si_{As}) antisite defects in CGA. For the native antisite acceptor, the hole appears to be delocalized in contrast to impurity antisites where the hole is mainly localized at the acceptor site. To estimate the location of the acceptor level in the band gap, we have computed the ionization potentials (IP) of the different antisite defects as well as of the self-embedding cluster. However, these values carry a large correlation error, since the IPs involve subtracting energies for systems with different numbers of electrons; for example, the band gap is estimated to be 1.58 eV, much higher than the experimental value. If we include a semi-empirical correlation correction to the IPs (i.e., the known correlation error for the calculations of the free atoms), the Ge antisite appears within the gap, with an IP of 0.36 eV with respect to the conduction band, while both C and Si appear within the conduction band, 0.09 and 0.71 eV respectively above its lower limit. The corrected gap value is 1.10 eV, still larger than the experimental value of 0.69 eV. If we further scale the energies to reproduce the experimental band gap, the resultant Ge antisite level comes out to be 0.226 eV. Although this value is still larger than the experimental 120-meV value for the shallow acceptor, we take this to be in good qualitative agreement. Clearly, carbon and silicon are not expected to form shallow acceptor states in this crystal.

Identification of Infrared Absorption Bands in ZnGeP_2 :

Three distinct photoinduced absorption bands were identified in ZnGeP_2 crystals (crystals provided by our industrial partner, BAE Systems in Nashua, NH). These absorptions are believed to be the cause of pump-induced absorption observed in devices. Two of these are associated with the singly ionized charge state of the zinc vacancy, the dominant defect in this material. These two bands occur at 1.2 microns and 2.2 microns. The other absorption band is associated with neutral phosphorus vacancies. The particular charge states of these native defects are manipulated using light, and results were correlated with photo-EPR studies. Phosphorus vacancies (donors) can compensate the Zn vacancies, changing their charge state and thus altering the absorption intensity.

Our work focused on the origin of the 2.2-micron band. The temperature and polarization dependences of this band have been determined. The absorption spectra taken at 10 K are shown in Fig. 14. The 2.2-micron band is highly polarized with $E \parallel c$ being the preferential absorbing direction. The intensity of the 2.2-micron band is very important to laser engineers, since ZnGeP_2 OPOs typically use pump sources operating near 2 microns. We have

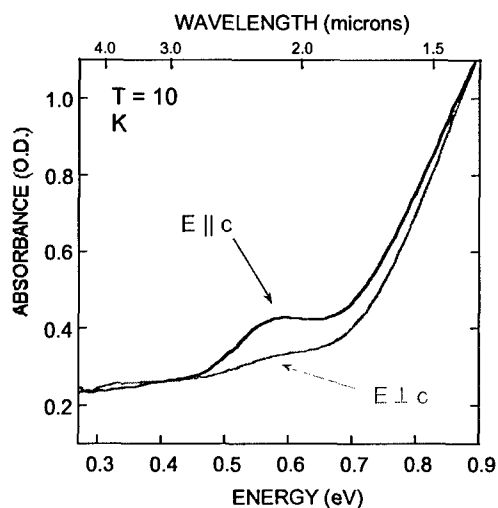


Figure 14. Optical absorption at 10 K in ZGP.

studied a series of crystals provided by BAE Systems and found that the intensity of the 1.2-micron and 2.2-micron bands are related. Our earlier work (Setzler et al., J. Appl. Phys. **86**, 6677 (1999)) showed that the 1.2-micron band is due to singly ionized Zn vacancies. We conclude that the 2.2-micron band also is due to that same defect. This is verified by the observed correlation in intensity of the 1.2-micron and 2.2-micron bands. To assign the 2.2-micron absorption to a particular transition, we have performed photo-induced EPR experiments using a semiconductor diode laser operating at 1.9 microns (can pump into the 2.2-micron band). We have monitored the intensity of the paramagnetic state of the Zn vacancy and we have noted that the 1.9-micron light reduces the concentration of singly ionized Zn vacancies while no other paramagnetic defect is created. This effect can only be observed at low temperatures ($T < 10$ K) and the EPR spectrum recovers its initial intensity as soon as the light source is shuttered. This result leads us to conclude that the 1.9-micron light is of sufficient energy to excite electrons from the valence band to the singly ionized Zn vacancy, thus converting the defect to the doubly ionized (nonparamagnetic) charge state.

Role of Copper as an Acceptor in ZnGeP₂:

Copper, substituting for zinc, is expected to provide an acceptor level in ZnGeP₂ that is shallower than the singly ionized zinc vacancy. Adding the Cu impurity to the lattice could thus lead to the elimination of absorption bands associated with the singly ionized Zn vacancy (a very important result for optimizing infrared countermeasure device performance). With our industrial partner BAE Systems, we have been investigating two types of copper-doped ZnGeP₂ crystals, those having copper incorporated during growth and those having copper diffused in after growth (i.e., in post-growth anneals). These samples were investigated using PL, PL excitation (PLE), and infrared absorption. A PL band at 1.3 eV at 5 K was observed. The temperature dependence of the 1.3-eV PL band gives a thermal activation energy of 0.11 ± 0.01 eV. PLE data show a resonance in intensity occurred at 0.1 eV below the conduction band when monitoring the 1.3-eV band. The 1.3-eV emission band is found to be unpolarized in contrast to PL bands observed in nominally undoped ZnGeP₂ crystals. The copper-diffused samples have an absorption band at 10 K peaking at about 0.62 eV. We suggest that the 1.3-eV luminescence band is donor-acceptor-pair recombination with the donor energy level about 0.1 eV below the conduction band and a Cu acceptor energy level about 0.62 eV above the valence band. This transition model is also supported by optical quenching experiments. Our work established that copper is not a shallow acceptor, as previously suggested. In separate studies, the EPR and ENDOR spectra from isolated copper acceptors have been observed and analyzed. They show that the neutral acceptor wavefunction has very little contribution from d-orbitals.

Effect of Doping with Group-VI Impurities in ZnGeP₂:

In order to compensate the large concentrations of Zn vacancies that occur in bulk crystals of ZnGeP₂, scientists at Air Force Research Lab (Wright-Patterson AFB) have suggested that intentional doping with donor impurities may be useful in converting all the Zn vacancies to the doubly ionized charge state. The doubly ionized charge state will then not participate in the near-infrared absorption. For this reason, it was important to understand the optical properties of donors in ZnGeP₂. The infrared absorption spectra from crystals doped with sulphur and selenium are shown below. The samples are about 3 mm in thickness. There is a new absorption band peaking near 0.3 eV which increases with illumination from either a HeNe laser (633 nm) or a Nd:YAG laser (1064 nm). The EPR spectrum due to the neutral sulphur donor ($S = \frac{1}{2}$) is shown in Fig. 16. The two curves in this latter figure are the EPR spectrum taken with the sample in the dark and the EPR spectrum taken after the sample has been illuminated with 633-nm light from a HeNe laser. Enhancement of the neutral donor EPR signal is observed.

Similar EPR results were obtained for Se doping. Illumination at low temperature forms an increased number of neutral donors (as detected by EPR), and this creates a new pathway for absorption. The electrons trapped at the

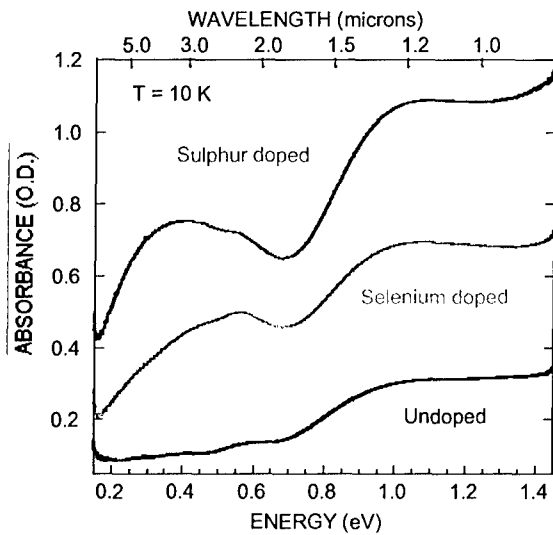


Figure 15. Infrared absorption showing effects of donor-doping on ZGP crystals.

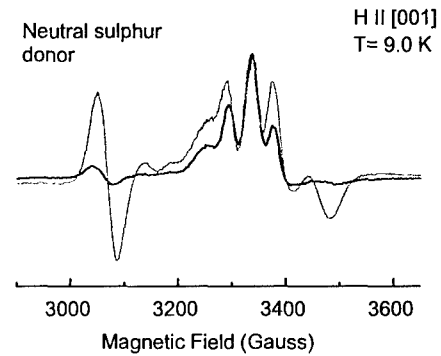


Figure 16. EPR before and after exposure to 633-nm light.

donor centers are excited into the conduction band. From these data, we determine the donor ionization energies for both S and Se in ZGP to be about 0.3 eV. Further evidence for the donor ionization energy was obtained using photoluminescence. A new PL band, at about 1.7 eV in doped crystals, was observed at 5 K. This new band is attributed to donor-hole recombination and requires a donor level at about 0.3 eV below the conduction band, because the band gap is 2 eV.

Correlation of Absorption and Luminescence in CdGeAs₂:

One of the limitations presently restricting use of CdGeAs₂ in nonlinear optical devices operating in the infrared is a room-temperature optical absorption peaking near 5.3 microns. Upon sample cooling, the absorption decreases. This absorption has been attributed to inter-valence band transitions and is associated with the presence of a shallow acceptor. Figure 17 shows absorption data taken at room temperature from three samples.

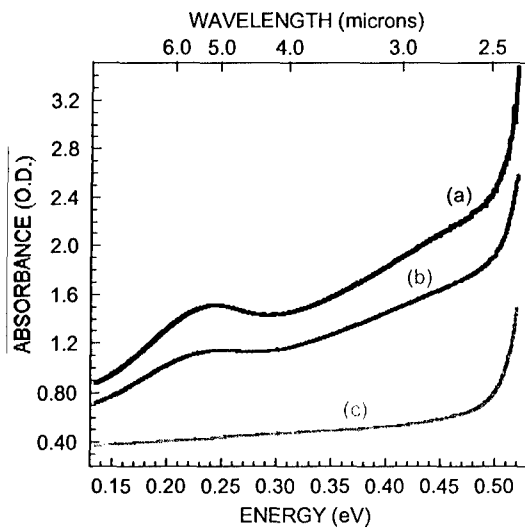


Figure 17. Optical absorption at room temperature from three CGA samples.

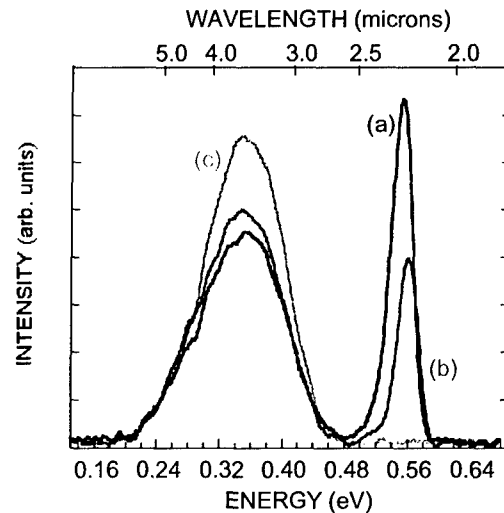


Figure 18. Photoluminescence at 10 K from the three different CGA samples used for Fig. 4.

We have studied a series of 38 CGA samples from BAE Systems representing a range of 5.3 micron absorption coefficient intensities from $\sim 0.1 \text{ cm}^{-1}$ to greater than 10 cm^{-1} . EPR, optical absorption, and infrared PL have been used to study these crystals. Among our findings are the following. The acceptorlike EPR signal at 10 K does not correlate directly with the 5.3 micron absorption band at room temperature. This suggests that the EPR spectrum represents a deeper acceptor. Recent analysis of its partially resolved hyperfine structure is consistent with the interaction of the unpaired spin with two equivalent Cd nuclei. A germanium-on-arsenic antisite defect would agree with these observations.

We observed two primary PL emission bands in our series of CGA crystals. These bands have peaks near 0.55 eV and 0.35 eV at 10 K. We find that the higher energy emission band is completely absent in crystals that show little or no absorption at 5.3 microns. We attribute this higher energy emission to the shallow acceptor defect. Even in the best undoped samples studied, we find the lower energy PL band is still present. The PL spectra corresponding to the three absorption curves of Fig. 17 are shown in Fig. 18. Note that the best sample in absorption has only the low-energy PL band.

A photoluminescence (PL) study has been performed at liquid-helium temperature on a set of over 50 p-type bulk single-crystal samples of CdGeAs_2 . As part of this study, the effect of surface preparation on PL emission was evaluated. Room-temperature optical absorption measurements that monitored the intensity of the intervalence band transition peaking near 0.22 eV (i.e., 5.5 μm) were compared with the low-temperature PL data. Every sample exhibited a PL band near 0.35 eV related to a deep acceptor. A second PL band near 0.55 eV was present in all of the samples having a large absorption band, but was observed in only a few samples with an absorption coefficient less than 3 cm^{-1} at 0.22 eV. We attribute this second band to donor-acceptor-pair recombination involving a shallow 120-meV acceptor and residual donor impurities. To produce low-absorption material for use in nonlinear optical devices, it is necessary to reduce the concentration of both acceptors or, alternatively, to dope with donor impurities that provide compensation.

A second PL study has been performed from 5 K to 200 K on a similar set of p-type bulk CGA single crystals. Within this large set of samples, the peak position of the emission band previously observed near 0.55 eV was found to vary from about 0.54 to 0.58 eV when using 1064-nm excitation with a power density of 2.5 W/cm^2 . These variations of the PL peak position with excitation power and sample temperature were measured and were found to be consistent with donor-acceptor pair (DAP) recombination in the presence of potential fluctuations. We found that the position of the DAP emission in a particular crystal depends on the hole carrier concentration and the level of compensation. Thermal quenching activation energies of 14 meV and 120 meV were determined for the donor and acceptor states, respectively. The acceptor defect involved in this radiative recombination is the primary center responsible for the commonly observed room-temperature absorption band at 5.5 μm in p-type CGA crystals. We believe that this acceptor is the Ge-on-As antisite.

Temperature Dependence of Polarized Absorption Bands in CdGeAs_2 :

For laser applications, it is important to understand the nature of the absorption bands in CGA crystals because they limit device performance. We have determined that there are at least four discrete absorption bands that occur within the 2 to 6 μm region in p-type CGA bulk crystals. The temperature and polarization behaviors of these absorption bands have been studied from 5 to 300 K. One band, peaking near 0.22 eV (5.5 μm), is the $V_2 \rightarrow V_1$ intervalence band transition (labeled band A below), and its intensity taken with $E \parallel c$ is about 2.8 times larger than that taken with $E \perp c$. Three additional absorption bands can be separately resolved below 200 K (see bands B, C, and D in left figure below). The broad band peaking near 0.38 eV is present only with $E \parallel c$. A second broad band peaking near 0.52 eV is detected using $E \perp c$. These two bands are transitions from the top two valence bands to a deep acceptor (most likely the Cd vacancy). A third absorption band peaking near 0.56 eV is detected using $E \parallel c$. This band is assigned to transitions from a shallow 120 meV acceptor (antisite Ge_{As}) to shallow donor states and/or conduction band states. At room temperature, the normally observed broad absorption feature extending from the band edge to beyond 0.2 eV is a result of the superposition of the four bands.

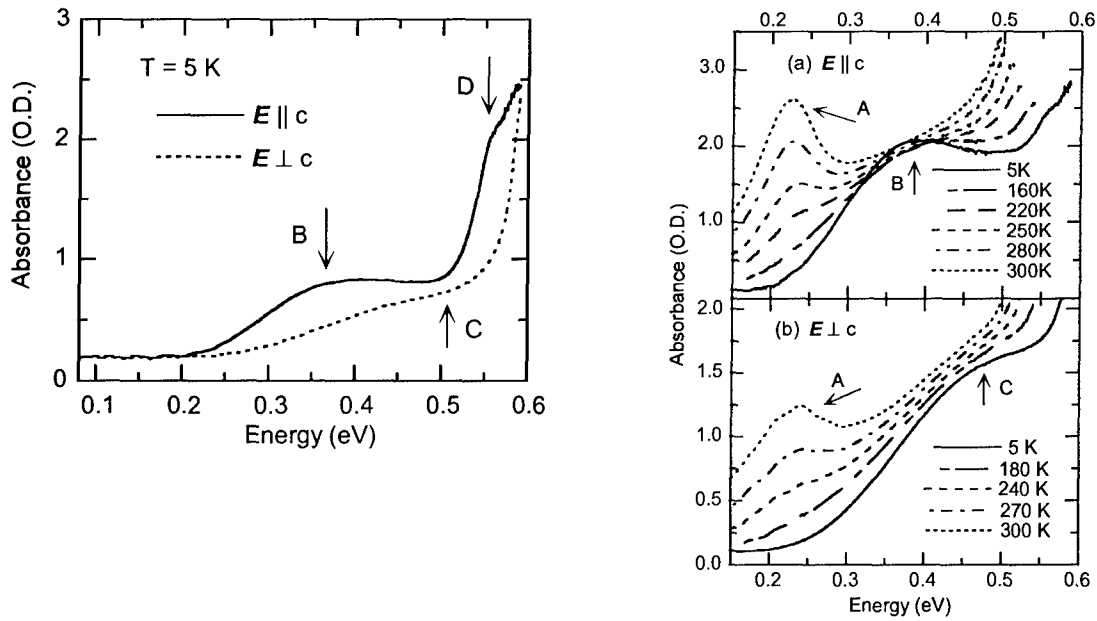


Figure 19. Polarized absorption data from p-type CGA sample at 5 K (left figure). Temperature dependence of absorption bands is shown at right.

Absorption at 2 Microns Due to Nickel Impurities in AgGaSe₂:

Because of its sufficient birefringence, high transmission, and large nonlinear optical coefficient, AgGaSe₂ is an attractive material for second harmonic generation (SHG) and optical parametric oscillator (OPO) applications in the mid-infrared. Optical absorption, electron paramagnetic resonance (EPR), and electron-nuclear double resonance (ENDOR) have been used to characterize Ni⁺ ions substituting for Ag⁺ ions in AgGaSe₂ crystals. These Ni⁺ ions are responsible for a strongly polarized optical absorption band peaking near 2.2 μm (the maximum absorption occurs with $E \parallel c$). Phonon structure is resolved at low temperature, fig. 20. This infrared band, which is present even in undoped crystals because of trace amounts of Ni, can significantly degrade the performance of optical parametric oscillators using AgGaSe₂. The optical absorption is shown below at room temperature (left figure) and low temperature (right figure).

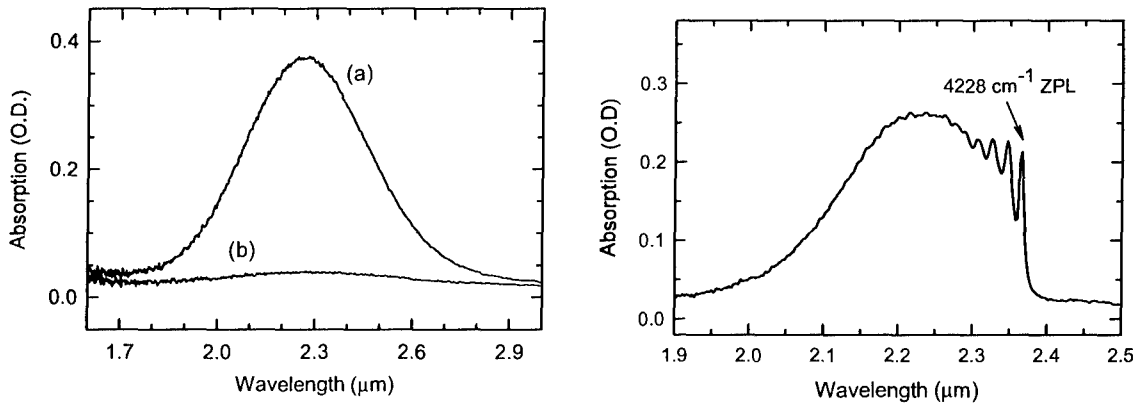


Figure 20. Polarized optical absorption from Ni⁺ ions in AgGaSe₂. (a) $E \parallel c$ and (b) $E \perp c$. These data were taken at room temperature with light propagating along the [100] direction. The sample thickness was 2.6 mm. Absorption at right taken at 10 K with unpolarized light propagating along the [100] direction. Phonon structure is observed at this temperature.

Sets of EPR and ENDOR angular dependence data were taken in the (010), ($\bar{1}10$), and (001) planes. This allowed the g matrix, the ^{61}Ni hyperfine and nuclear quadrupole matrices, the ^{77}Se hyperfine matrix for the four nearest neighbors, and the $^{69,71}\text{Ga}$ hyperfine and nuclear quadrupole matrices for four neighbors to be determined. Of the eight gallium near neighbors, only the four in the basal plane containing the Ni^+ ion have a significant interaction. Large hyperfine interactions with $^{107,109}\text{Ag}$ nuclei were not observed. The EPR and ENDOR data provide an accurate identification of the defect.

Improved Optical Transparency in Chromium-Doped CdGeAs_2 :

The two distinct cations in the chalcopyrite crystal structure offers a unique opportunity to study the different charge states of transition-metal ions. This will have ramifications for the optical absorption (as compensators for native defects) and for potential spintronic devices (the magnetic ion itself may be electrically active, i.e., an acceptor or donor). We used electron paramagnetic resonance (EPR) to investigate chromium ions in single crystals of CGA grown by the horizontal gradient freeze technique at Stanford University and BAE Systems. Signals from Cr^{2+} and Cr^{4+} ions were observed near 12 K. The Cr^{2+} ions have the $3d^4$ configuration with $S = 2$ and substitute at the Cd sites, while the Cr^{4+} ions have the $3d^2$ configuration with $S = 1$ and substitute at the Ge sites. Thus, each impurity represents a neutral center. We did not observe signals from Cr^{3+} , nor were the two observed signals photoactive. The two EPR spectra both display the tetragonal symmetry of the lattice, which suggests that these centers are not perturbed by nearby defects. The ratio of Cr^{2+} and Cr^{4+} in a particular CGA crystal depends on the growth conditions and stoichiometry. Improved transparency of the crystals was observed with increasing Cr^{2+} . The absorption was not seen to depend on Cr^{4+} .

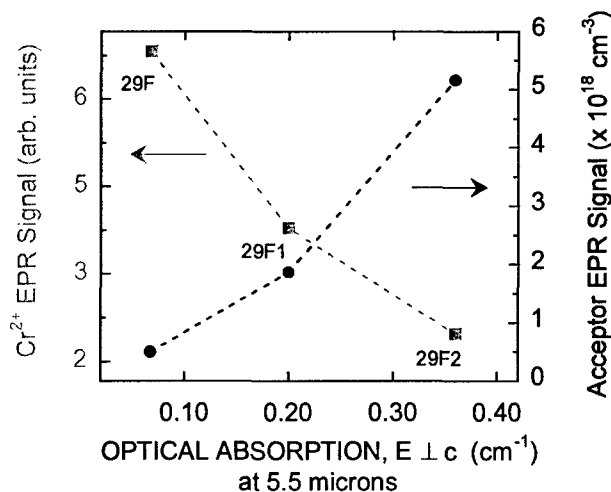


Figure 21. Reduction in optical absorption was achieved (accompanied by reduced native acceptor EPR signal) with increased incorporation of Cr^{2+} ions in CGA samples.

Characterization of Mn-doped ZnGeP_2 :

Numerous investigators have suggested that Mn-doped ZnGeP_2 crystals may be suitable for spintronic applications. We have used EPR and electron-nuclear double resonance (ENDOR) to characterize isolated Mn^{2+} ($3d^5$) ions in a bulk ZnGeP_2 crystal grown by the horizontal Bridgman technique. The Mn^{2+} ions substitute for the Zn^{2+} ions in this tetragonal chalcopyrite lattice. There were no signals from Mn^{3+} or Mn^{4+} ions. From the Mn^{2+} EPR data, we obtained principal values for the g matrix and values for the a, F, and D crystal-field parameters. The two equivalent sites occupied by the Mn^{2+} ions are related by a "twist" angle of 5.6° (this angle describes the small clockwise and counterclockwise rotations of the MnP_4 units about the unique [001] crystal axis). ENDOR signals from the ^{55}Mn nuclei gave hyperfine and nuclear electric quadrupole parameters. Principal values and principal-axis directions for the four nearest-neighbor ^{31}P nuclei were also obtained from ENDOR spectra. Doublets observed in these latter spectra are attributed to indirect nuclear-nuclear interactions. These results demonstrate that the wave function of the Mn^{2+} ion is very localized.

Characterization of Mn-doped CdGeAs₂

Electron paramagnetic resonance (EPR) and electron-nuclear double resonance (ENDOR) techniques have been used to characterize Mn²⁺ (3d⁵) ions in CdGeAs₂ crystals. The crystals were grown at Stanford University and the characterization studies were performed at WVU. One of the Mn-doped CdGeAs₂ crystals was sent to BAE Systems where it was carefully aligned by K. Zawilski using their x-ray Laue apparatus. Thus, a complete set of angular-dependent ENDOR data could be taken. The Mn-doped CGA samples were p-type with room-temperature hole concentrations ranging from $2 \times 10^{15} \text{ cm}^{-3}$ to $5 \times 10^{16} \text{ cm}^{-3}$. The Mn²⁺ ions substitute for the Cd²⁺ ions in this tetragonal chalcopyrite lattice, and form “deep” isoelectronic centers. Their g values and crystal-field parameters were found to be $g_{\parallel} = 2.0025$, $g_{\perp} = 2.0011$, $D = 118.8 \text{ MHz}$, $a + \frac{2}{3}F = 18.4 \text{ MHz}$, and $a = -0.3 \text{ MHz}$. The hyperfine and nuclear electric quadrupole parameters obtained from the ⁵⁵Mn ENDOR spectra are $A_{\parallel} = -154.94 \text{ MHz}$, $A_{\perp} = -155.69 \text{ MHz}$, and $P = 0.622 \text{ MHz}$. No evidence was found that any of the Mn impurities become Mn⁴⁺ and substitute for Ge⁴⁺. Crystalline CdGeAs₂ is an excellent candidate for spintronic applications requiring ferromagnetic behaviour at room temperature. Large concentrations of Mn²⁺ ions can easily be incorporated on the Group II site in this material and crystals can be grown (independent of their level of Mn doping) as either p-type or n-type with large carrier concentrations at room temperature. These properties suggest that Mn-doped CdGeAs₂ should exhibit carrier-mediated ferromagnetism (i.e., magnetic ordering resulting from the exchange interaction between localized magnetic spins and delocalized carriers). The results of this study appeared in *Physica Status Solidi B* (online in Sept. 2006).

Characterization of Zinc Vacancy in ZnGeP₂

The singly ionized zinc vacancy is associated with the dominant absorption band limiting the application of ZGP crystals in directed infrared countermeasure (DIRCM) devices. Reduction of the concentration of this particular defect during growth or by post-growth treatments has provided ZGP crystals having improved device performance. A recent theoretical study by Walter Lambrecht (Case Western Univ.) published in *Physical Review B* has raised questions about the local symmetry and wave function of the singly ionized Zn vacancy defect. A severe limitation of these calculations is the size of the supercell used to replicate the point defect and surrounding lattice. In order to provide a complete description of the lattice relaxation and the extent of the wave function overlap onto the surrounding P neighbors, we are performing additional EPR and ENDOR measurements on ZGP samples provided by BAE Systems.

The ENDOR-induced EPR technique (EI-EPR) is being used to precisely determine the g matrix (i.e., principal values and directions) for the singly ionized zinc vacancy in ZnGeP₂. Previous EPR measurements taken at three high-symmetry directions of the magnetic field had provided an approximate g matrix. Broad and strongly overlapping EPR signals did not allow a precise g matrix to be determined from EPR alone. The EI-EPR technique gives much higher resolution, since only the EPR signals associated with one orientation of the defect (of the four possible) are present in a particular spectrum. A complete set of EI-EPR data has been taken for the singly ionized Zn vacancy and is presently being analyzed. The EI-EPR capability was added during the past year to the magnetic resonance laboratory at WVU, thus permitting these experiments to be performed on ZGP. Also, ENDOR data have been acquired to completely map out the interactions with the ten closest ³¹P neighbors. Together, these results will provide the stringent tests for defect wave functions generated from ab initio calculations.

Photoluminescence of n-type Indium-Doped CdGeAs₂

N-type CdGeAs₂ samples were grown at Stanford University and at BAE Systems and provided to WVU for optical and electrical characterizations. Normally, undoped CGA is p-type due to two native acceptors, one shallow and one deep. Donor doping would be an attractive and cost-effective solution to improving CGA performance in laser devices if the acceptor states could be compensated and a minimum of free carriers produced at the device operating temperatures. We completed studies of CGA boules that were intentionally doped with indium, selenium, or tellurium impurities. Samples cut from these boules and oriented using x-ray Laue were provided to WVU for characterization using photoluminescence (PL) and Hall-effect measurements. A near-edge PL band from heavily In-doped CdGeAs₂ samples shifts to higher energy and becomes broader with increasing electron concentration. The observed shifts in peak energies were compared to predictions for donor-acceptor pair and free-to-bound (electron-acceptor) recombinations including band-filling, band-tailing, and band-gap shrinkage effects due to the

high doping levels. As part of our reported analysis (J. Phys. Condensed Matter **17**, 5687 (2005)), an expression was derived for the nonparabolicity coefficient (α) for compounds with nonzero crystal-field splitting. The value of α is 0.776 for CGA, as compared to 0.816 for the zinc-blende GaAs. Excellent agreement between the PL emission peak energy and the predicted energy for electron-acceptor was found when the conduction band nonparabolicity was included. In indium-doped CGA samples with $n > 2 \times 10^{18} \text{ cm}^{-3}$, the free-to-bound PL transition related to a shallow 120-meV acceptor level is still dominant. The indium donors compensate and do not eliminate the shallow acceptor defects. A significant finding from our study was that the lower energy PL band due to deep acceptors was suppressed. This suggests that the deep acceptor may be a Cd vacancy, and thus doping on the Cd site with a donor impurity not only provides compensation for any existing acceptor states, but has also suppressed formation of the deep native acceptor defect.

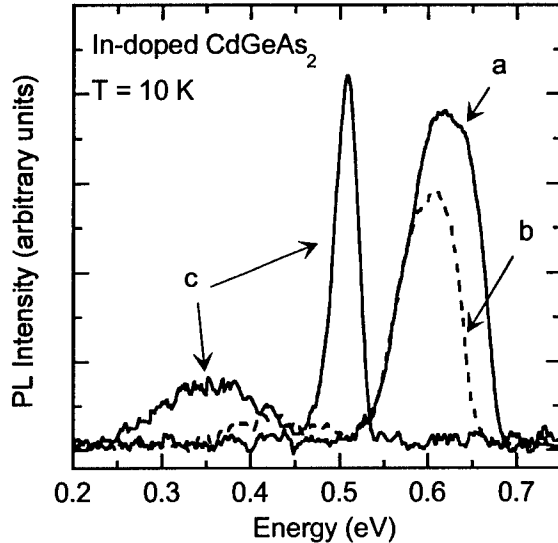


Figure 22. PL spectra taken at 10 K for three n-type CdGeAs₂ samples: sample a ($n = 4.3 \times 10^{18} \text{ cm}^{-3}$), sample b ($n = 2.7 \times 10^{18} \text{ cm}^{-3}$), and sample c ($n = 4.6 \times 10^{17} \text{ cm}^{-3}$). Carrier concentrations were obtained from Hall measurements at 300 K.

Photoluminescence of n-type Group-VI-Doped CdGeAs₂:

Doped CGA samples using Group-VI impurities were also provided for our study. Donor doping using Se or Te on the anion site suppressed the shallow acceptor (the Ge-on-As antisite). No PL was observed that could be assigned to the shallow acceptor in n-type samples doped with Se or Te with room-temperature free-carrier concentrations in the range from $n \sim 10^{16} - 10^{17} \text{ cm}^{-3}$. The deep acceptor was, however, still present. This supports the assignment of a Cd vacancy for this deep center. Photoluminescence from low-absorption, improved CdGeAs₂ crystals doped with Se or Te is shown in the figure below. Only the low-energy emission band is present. No evidence of the presence of the shallow Ge_{As} acceptor is observed.

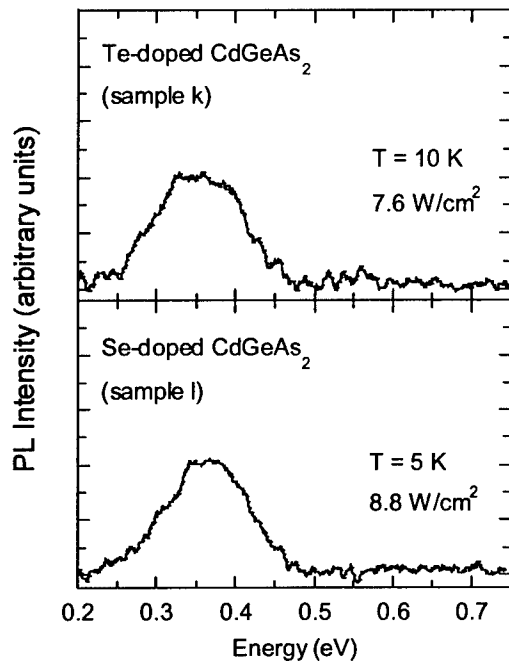


Figure 23. PL spectra from n-type CdGeAs₂ doped with Te or Se.

Effects of Free Carriers in n-type CdGeAs₂:

Room temperature infrared absorption and reflectance experiments have also been completed on n-type CdGeAs₂ bulk samples doped with indium. Incorporation of indium into CGA typically yields material that is “overdoped” and free-carrier absorption renders the samples unsuitable for infrared laser devices. The magnitude of the free-carrier absorption in these samples followed a λ^p dependence, where p varies from 3 to 3.5, as expected for impurity scattering. A correlation between the free-carrier absorption coefficient at 5 μm and the room-temperature carrier concentration (from Hall measurements) was established for n_{H} in the range from $2 \times 10^{17} \text{ cm}^{-3}$ to $4 \times 10^{18} \text{ cm}^{-3}$. The dependence of the free-carrier relaxation time τ on carrier concentration was extracted from the electrical data, and the variation in τ was used in our analysis of the optical absorption data. Infrared reflectance data for these n-type samples was also used to relate the plasma minimum with optical effective masses (m_{opt}^*). Our previous result for the conduction-band nonparabolicity was used in the prediction for variation in effective mass m^* with carrier concentration, n . Experimental results followed theoretical predictions: free carrier absorption coefficient, $\alpha_f \sim n^2(m^*)^{-1.5}$. Our studies establish a complete understanding of the optical and electrical behaviors for n-type indium-doped CGA (appears in J. Phys.: Condensed Matter **18**, 2741 (2006)).

1e) Birefringently phasematched AlGaAs nanostructures – preparation, characterization and testing

The aluminum gallium arsenide/aluminum oxide (AlGaAs/Al_xO_y) material system is very attractive for non-linear optical applications, because of the large nonlinear susceptibility (d_{14} of GaAs = 90pm/V), the high index contrast, the mature device fabrication technologies and the possibility of integrating passive and active devices on the same substrate. Since AlGaAs is not birefringent, different techniques to solve the problem of phasematching have been developed in the past. AlGaAs quasi-phasematched or artificially birefringent waveguides have already been demonstrated; however, either they require a complex fabrication process or the conversion efficiency remains relatively low due to the poor lateral confinement. We have developed tightly confining nonlinear waveguide and cavity devices, ultra-compact and with an extremely high normalized conversion efficiency.

Recently, we have re-designed our previous device geometry in order to achieve phasematching by artificial birefringence. This approach resulted in the highest normalized conversion efficiency reported, to our knowledge, ~20x higher than in previously reported works. This is accomplished by simply inserting a layer of low-index material (Al_xO_y) in the AlGaAs waveguide core. This thin Al_xO_y layer in the core does not significantly affect the (TE) mode profile at the fundamental wavelength, but lowers significantly the effective index of the (TM) mode at the second harmonic (type II phasematching). In this way, phasematching is achieved at a specific wavelength, which is adjustable by varying the waveguide width (typically between 800 and 1000 nm). The normalized conversion efficiency for this structure is ~ 20,000 %/W/cm², more than two orders of magnitude higher than the efficiency of LiNbO₃ nonlinear waveguides. Moreover, this structure does not require multiple MBE growths and can be fabricated in a few steps, i.e. e-beam lithography, hard mask transfer by chrome evaporation and liftoff, chlorine plasma etching, mask removal and thermal oxidation. The RMS roughness of fabricated waveguides, measured by SEM inspection, is less than 6 nm over a few microns of length, and less than 30 nm over 600 μm (the length of our samples) and is sufficiently small to maintain the phasematching condition.

The loss coefficient at the fundamental waveguide (measured by the Fabry-Perot method) is estimated to be $\sim 2.3 \pm 0.7 \text{ dB/mm}$. We used the SHG tuning curve (figure 24a) to estimate the second harmonic (SH) loss. The SH loss of 25-35 dB/mm is currently the limiting factor to the conversion efficiency, experimentally found to be 4-5%/W. The large uncertainty in loss is due to uncertainty in collection efficiencies of the first harmonic (FH) and SH. The high loss at the second harmonic originates from surface roughness in the device. In fact, a crude estimation based on the amount of field at the interfaces indicates that the SH loss due to roughness at the horizontal interfaces could be 40-70x larger than the FH loss, for the same amount of roughness. Moreover, the SH mode would be 500-900x more sensitive to roughness at the horizontal interfaces than at the sidewalls. Thus, only a small amount of roughness at the horizontal interfaces (due, for example, to the thermal oxidation) could be sufficient to explain such a SH high loss coefficient.

The high SH loss is currently the limiting factor to the efficiency of our waveguides. A way to reduce the effect of high loss and to further enhance the conversion efficiency is to build a resonant cavity embedded in the waveguide. We have also designed and fabricated a waveguide-embedded cavity, resonant at the fundamental wavelength. This

cavity should enhance the nonlinear conversion efficiency by a factor $\sim F^2$, where F is the finesse of the cavity. According to FDTD simulations, the novel mirror (figure 24b) has the characteristic of reflecting the fundamental wavelength (1550 nm) and being completely transparent at the second harmonic (775 nm). This behavior is usually very difficult to obtain in conventional waveguide mirrors, due to very high loss at the second harmonic. Tapered ends of the mirror reduce the mode mismatch losses and increase the reflectivity.

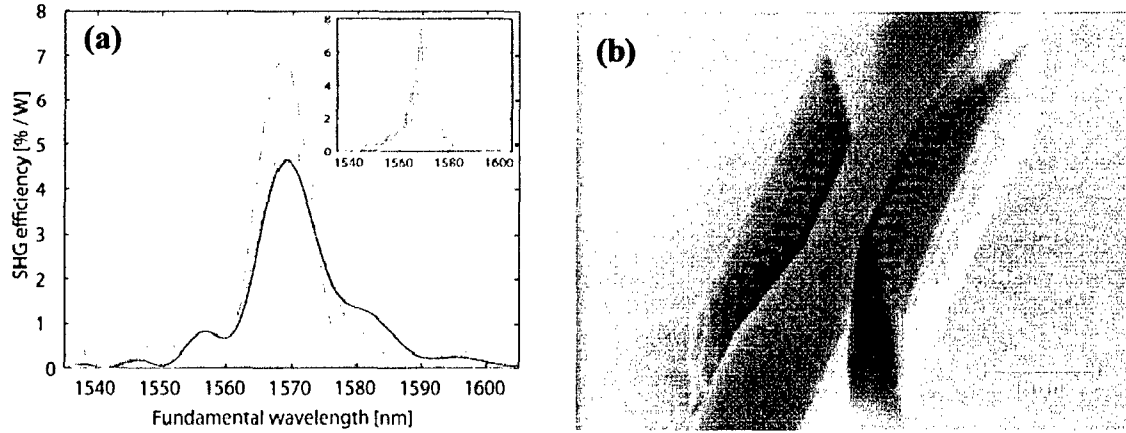


Figure 24. (a) Experimental efficiency (light/blue solid) calculated by normalizing the output SH power to the squared output fundamental power and fitted efficiency with (black solid) and without (pink dashed) taking into account drift of the effective index; Inset: SH power normalized by the input fundamental power. Note the modulation due to the Fabry-Perot fringes at the fundamental wavelength. (b) SEM picture of fabricated mirror.

Using this mirror, we observed a total cavity enhancement of ~ 5.3 and a total efficiency 50% larger than the highest efficiency achievable with a plain waveguide. These cavities constitute only a proof of concept and not optimal devices. FH spectra of other samples suggest greater than 10x enhancements, which would yield, with the correct layer structure, efficiencies as high as 15%/W. We estimate that, given the actual loss, simply by optimizing the geometrical parameters of the cavity, enhancements greater than $\sim 18x$ (corresponding to efficiencies as high as 38%/W) should be achievable. Furthermore, we can speculate that, if the FH propagation losses of the waveguide and mirror could be lowered by a factor ~ 10 (e.g., by improving the quality of the MBE grown crystal or with smoothing-etch techniques), assuming the actual SH loss, enhancements of over 200x should be achievable, with efficiencies as high as 1600%/W, comparable to the efficiency of commercial devices (e.g. 1400%/W for 6.45-cm-long LiNbO₃ waveguides).

1f) Application of orientation-patterned GaAs for generation of terahertz radiation

Sources of electromagnetic radiation with terahertz (THz) frequencies have been actively investigated during the last decade for applications in imaging and spectroscopic sensors. Femtosecond optical pulses have been shown to efficiently generate THz waves in quasi-phased-matched (QPM) gallium arsenide (GaAs) [1]. Related work at Stanford on THz generation has been supported principally with DARPA funding through AFOSR under FA9550-04-1-0465. However, the THz project did receive indirect facilities support related to the growth of OP-GaAs from the MURI program, and a small amount of direct salary support related to the application of OP-GaAs devices from the MURI program, as well. In the THz program, we demonstrated a picosecond system creating a near-diffraction-limited THz source with 1 mW of average power, an optical-to-optical efficiency of 0.01%, and a tunable frequency from 0.65 – 3.4 THz in QPM GaAs. Our approach was based on intracavity difference-frequency mixing in QPM GaAs of the signal and idler waves of a near-degenerate type-II MgO:PPLN OPO synchronously pumped with a CW-modelocked solid-state IR laser. GaAs is attractive for this application due to its large nonlinear coefficient as well as low THz absorption.

The 1064 nm source pumped a type-II PPLN crystal, in which orthogonally polarized signal and idler waves were generated near 2100 nm and 2150 nm, respectively. In the synchronously-pumped doubly-resonant oscillator

(DRO), both the signal and idler waves resonated inside a low-loss optical cavity, generating large intracavity powers, resonantly enhancing the difference frequency generation of the THz output power, which is proportional to the product of signal and idler powers [2]. The SP-OPO employed a novel offset cavity configuration, which avoided the “DRO mirror” back-conversion problem generally present in linear DRO cavities (Fig. 25). The thin film plate polarizers separated the orthogonally polarized signal and idler waves, allowing for independent control of the length of the cavity for the signal and idler waves. By placing a piezoelectric actuator on one cavity end mirror and using optical power leaking through a highly-reflecting cavity mirror, a dither-and-lock control system is planned to stabilize the length of both cavities.

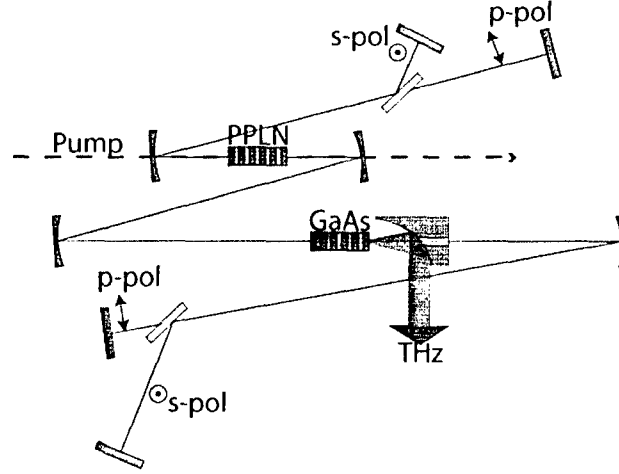


Figure 25. Doubly resonant synchronously pumped-OPO offset cavity design with THz wave out-coupling.

THz generation through signal and idler difference frequency generation (DFG) requires nearly-degenerate phasematching. Type-II QPM PPLN creates orthogonally polarized signal and idler waves which allows operation through degenerate phasematching as shown in Figure 26a where by convention the idler is the longer wave.

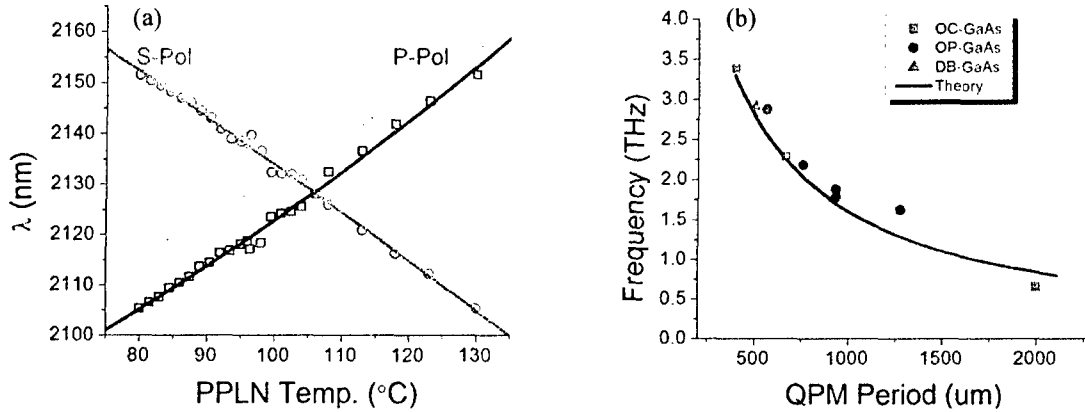


Figure 26. (a) Temperature tuning curves of Type II QPM PPLN. (b) THz frequencies generated in QPM OC-GaAs, OP-GaAs, and DB-GaAs.

By changing the temperature of the PPLN crystal, we can tune the wavelengths of the signal and idler waves and thus their THz difference frequency. The generated THz waves spanned 0.65 – 3.4 THz by engineering varying

QPM gratings in OC-GaAs (optically contacted), OP-GaAs (orientation patterned), and DB-GaAs (diffusion bonded). Figure 26b shows that measured THz frequencies follow QPM theory.

When the nonlinear gain is large enough the THz wave mixes with the idler to create a second red-shifted idler (satellite) and another wave at the same THz frequency. This process continues between the THz wave and subsequent satellites, and each process adds additional energy to the THz wave increasing the optical conversion efficiency. Figure 27 shows the signal and idler resonating inside the OPO and two measured satellites. Each wave of Figure 27 is normalized to unity to illustrate correct spacing and excellent lineshape. The signal and 1st satellite are horizontally polarized, and the idler and 2nd satellite are vertically polarized, as expected from the symmetry of the nonlinear susceptibility tensor of GaAs.

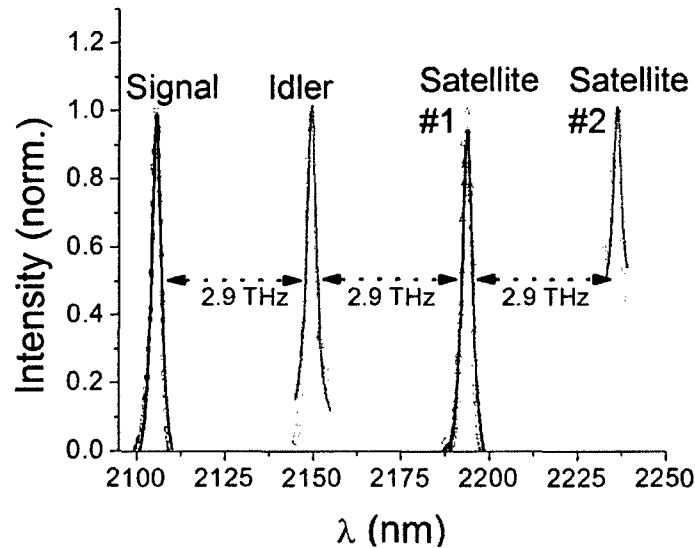


Figure 27. Signal, idler, and two satellites created by cascading in DB-GaAs.

Currently, 1 mW of average THz power is created in diffusion-bonded gallium arsenide (DB-GaAs) with a frequency of 2.9 THz in 100 μ s bursts of 50-MHz-repetition rate pulses. We believe that the duration of these bursts is limited by self-heating in the high-loss sample of DB-GaAs currently available. Future work will include maintaining DRO operation at 1 mW of average THz power utilizing a dither-and-lock length-stabilizing control system. Larger signal and idler beams inside GaAs and less mid-IR GaAs absorption will reduce the effect of nonlinear refraction and allow higher circulating powers for a given pump power. Both considerations will increase the efficiency of THz generation. Use of cascading to further increase the THz conversion efficiency will be explored.

[1] K. L. Vodopyanov, M. M. Fejer, Y.-S. Lee, W. C. Hurlbut, V.G. Kozlov, Terahertz wave generation in quasi-phase-matched GaAs, *Appl. Phys. Lett.*, 89, 141119 (2006).

[2] Y.R. Shen: *The Principles of Nonlinear Optics*, Wiley, New York, (1984).

2) Experiments involving magnetic chalcopyrite and other semiconductors for potential Spintronic applications

Ferromagnetism with a transition temperature of 325 K and a coercive force $H_c = 220$ Oe (at 300 K) was observed in thin films of the chalcopyrite semiconductor MnGeP_2 . Extensive transport measurements were performed on MBE-grown thin films of MnGeP_2 . The observation of a field-saturable anomalous Hall effect *with accompanying hysteresis*, along with direct magnetization measurements, confirmed that the material is ferromagnetic with a Curie temperature of 325K. Curiously a field-saturable component is present above the Curie temperature, where magnetization measurements show the material to be paramagnetic. Often a field saturable Hall component is offered as evidence for ferromagnetism and a significant result of our observation is that without an accompanying hysteresis ferromagnetism cannot be unambiguously confirmed from a field-saturable Hall effect

Artificial superlattices of the compounds MnAs/GaAs, MnAs/Ge MnAs/Si and Mn/Ge were prepared by MBE; all show room-temperature ferromagnetism with a Curie temperature above that of MnAs (318K); the latter is metallic, but as a short-period superlattice with Si, Ge, and GaAs shows semiconducting behavior.

MnAs is a ferromagnetic, but metallic, semiconductor with a transition temperature of 318K and a coercive force $H_c = 220$ Oe (at 300 K). Interestingly, as an artificial superlattice alternated with GaAs it can have a higher Curie temperature of 325K. Moreover, the electrical-transport properties change from metallic to semiconducting on decreasing the total thickness from 300 to 20 nm for MnAs/GaAs(001) samples. These variations of the magnetic and electrical-transport properties are thought to be caused by a substrate-induced strain.

Ferromagnetic multilayers consisting of non-magnetic Si and ferromagnetic MnAs, i.e. Si/MnAs multilayers, were grown on (001) GaAs by molecular beam epitaxy. It was found that a Si(1nm)/MnAs(0.5nm) multilayer holds ferromagnetic ordering up to high temperatures (>400K). A coercive field of 344 Oe at 300K is obtained from hysteresis loop measurements.

We successfully fabricated MnAs/Ge multilayer structures using molecular beam epitaxy. These multilayers were grown on (001) GaAs substrates at a growth temperature of 580C. The MnAs/Ge multilayer with a 100 Å period thickness exhibited ferromagnetism up to 345K with a coercive field of 147 Oe at 300K and a vanishingly small in-plane magnetic anisotropy, as determined from temperature-dependent SQUID magnetization and hysteresis loop measurements.

A series of copper-doped zinc oxide films were grown by pulsed-laser ablation. Films grown under conditions that produced n-type ZnO were nonmagnetic while those grown under conditions that produced p-type were ferromagnetic with a Curie temperature above 350 K. The magnetic moment per copper atom decreased as the copper concentration increased. An explanation for this result is proposed based on the distance between nearest-neighbor copper atoms.

GOVERNMENT SITE REVIEWS AND GOVERNMENT PARTICIPANTS:

19 June 2001 – Stanford University, Chalcopyrite MURI Kickoff Meeting. Full-day technical meeting attended by Major Dan Johnstone (AFOSR), Dr. K. Schepler (AFRL/WPAFB), Capt. Eric Blasch (AFOSR/WPAFB), Dr. Shekhar Guha (AFRL/MLPJ), Dr. Shashi P.Karna (AFRL/Kirtland AFB), Dr. D. Bliss (AFRL/Hanscom AFB) Dr. P. Schunemann (BAE Systems) and Dr. K. Vodopyanov (Stanford University).

18 Sept. 2003 – Stanford University (in conjunction with Stanford Photonics Research Center Annual Meeting). Full-day technical review attended by Lt. Col. T. Steiner (AFOSR), Dr. K. Schepler (AFRL), Dr. N. Fernelius (AFRL), Dr. T. Kulp (Sandia National Lab), Dr. S. Bisson (Sandia National Lab.).

CUMULATIVE PUBLICATIONS SUPPORTED BY MURI:

1 a,b,c) Orientation-patterned GaAs and GaP for nonlinear optical applications Stanford (Fejer/Byer/Harris)

“All-epitaxial fabrication of thick, orientation-patterned GaAs films for nonlinear optical frequency conversion,” L.A. Eyres, P.J. Tourreau, T.J. Pinguet, C.B. Ebert, J.S. Harris, M.M. Fejer, L. Becouarn, B. Gerard, and E. Lallier, *Appl. Phys. Lett.* **79**, 904-906 (2001).

“All-epitaxial orientation-patterned semiconductors for nonlinear optical frequency conversion”, L. A. Eyres, PhD Thesis, Stanford University, December 2001.

“Difference frequency generation of 8-μm radiation in orientation-patterned GaAs”, O. Levi, T.J. Pinguet, T. Skauli, L.A. Eyres, K.R. Parameswaran, J.S. Harris, M.M. Fejer, T.J. Kulp, S.E. Bisson, B. Gerard, E. Lallier, L. Becouarn *Opt. Lett.* **27**, 2091-2093 (2002).

"Measurement of nonlinear coefficient of orientation-patterned GaAs and demonstration of highly efficient second harmonic generation", T. Skauli, K. L. Vodopyanov, T. J. Pinguet, A. Schober, O. Levi, L.A. Eyres, M. M. Fejer, J. S. Harris, B. Gerard, L. Becouarn, E. Lallier, *Opt. Lett.* **27**, 628-630 (2002).

"Template design and fabrication for low-loss orientation-patterned nonlinear AlGaAs waveguides pumped at 1.55 μm ," X. Yu, L. Scaccabarozzi, O. Levi, T. J. Pinguet, M. M. Fejer, and S. Harris, *J. Crys. Growth* **251**, 794-799 (2003).

"Improved dispersion relations for GaAs and applications to nonlinear optics," T. Skauli, P. S. Kuo, K. L. Vodopyanov, T. J. Pinguet, O. Levi, L. A. Eyres, J. S. Harris, M. M. Fejer, B. Gerard, L. Becouarn, and E. Lallier, *J. Appl. Phys.* **94**, 6447-6455 (2003).

"Optical parametric oscillation in quasi-phasematched GaAs", K. L. Vodopyanov, O. Levi, P. S. Kuo, T. J. Pinguet, J. S. Harris, M. M. Fejer, B. Gerard, L. Becouarn, E. Lallier, *Opt. Lett.* **29**, 1912-1914 (2004).

"Single-phase growth studies of GaP on Si by solid-source molecular beam epitaxy," X. J. Yu, P. S. Kuo, K. Ma, O. Levi, M. M. Fejer, and J. S. Harris, *J. Vac. Sci. Technol. B* **22**, 1450-1454, (2004).

"Optical parametric oscillator based on microstructured GaAs," K. L. Vodopyanov, O. Levi, P. S. Kuo, T. J. Pinguet, J. S. Harris, M. M. Fejer, B. Gerard, L. Becouarn, and E. Lallier, *Proc. SPIE* **5620**, 63-69 (2004).

"Efficient continuous wave second harmonic generation pumped at 1.55 μm in quasi-phase-matched AlGaAs waveguides," X. Yu, L. Scaccabarozzi, J. S. Harris, P. S. Kuo, and M. M. Fejer, *Optics Express* **13**, 10742-10753 (2005).

"MBE Growth of III-V Materials with Orientation-patterned Structures for Nonlinear Optics," X. Yu, Ph.D. thesis, Stanford University, March 2006.

"Optical parametric generation of a mid-infrared continuum in orientation-patterned GaAs," P. S. Kuo, K. L. Vodopyanov, M. M. Fejer, D. M. Simanovskii, X. Yu, J. S. Harris, D. Bliss, and D. Weyburne, *Opt. Lett.* **31**, 71-73 (2006).

Presentations

"Broadband Continuum Generation in GaAs (Invited)," Paulina S. Kuo, K. L. Vodopyanov, D. M. Simanovskii, X. Yu, M. M. Fejer, J. S. Harris, D. Bliss, D. Weyburne, in Conference on Lasers and Electro-Optics/Quantum Electronics and Laser Science 2006 (Optical Society of America, Washington, DC, 2006), paper CThG4.

"Fabrication of low loss quasi-phase matched nonlinear AlGaAs waveguide pumped at 1.55 μm ," X. Yu, L. Scaccabarozzi, P. S. Kuo, M. M. Fejer, J. S. Harris (Presented at NAMBE 2005, Santa Barbara, CA, Sept, 2005).

"Growth Studies of Single Phase GaP on Si by Solid-source MBE," Xiaojun Yu, Paulina S. Kuo, Martin. M. Fejer and James S. Harris, Jr., (Presented at the 2004 spring MRS meeting, San Francisco, CA, April 11 – 16, 2004).

"Long-wave infrared chemical sensing based on orientation-patterned GaAs," S. E. Bisson, T. J. Kulp, O. Levi, J. S. Harris, and M. M. Fejer, CLEO/IQEC and PhaST Technical Digest on CD-ROM (Optical Society of America, Washington, DC, 2004), paper CMN1.

"Long-Wavelength Infrared Chemical Sensing (Invited)," Scott Bisson in Conference on Lasers and Electro-Optics/Quantum Electronics and Laser Science 2006 (Optical Society of America, Washington, DC, 2006), paper CWA4.

"Orientation-patterned GaAs and Its Applications (Invited)," Martin M. Fejer, in Conference on Lasers and Electro-Optics/Quantum Electronics and Laser Science 2005 (Optical Society of America, Washington, DC, 2005), paper CThQ1.

"Single phase growth studies of GaP on Si by Solid-source MBE," X. Yu, P.S. Kuo, K. Ma, O. Levi, Prof. M. M. Fejer and Prof. J.S. Harris, Jr. (Presented at NAMBE 2003, Keystone, CO, Sep 29 – Oct 2, 2003).

"Template design and fabrication for low loss orientation-patterned nonlinear AlGaAs waveguides pumped at 1.55 μm ," X. Yu, L. Scaccabarozzi, T. J. Pinguet, O. Levi, M. M. Fejer and J. S. Harris, (Presented at the International MBE Conference XII, San Francisco, CA, Sept. 2002).

"Thermo-optic characterization of GaAs for quasi-phase-matched nonlinear-optical applications," T. Skauli, P. S. Kuo, K. L. Vodopyanov, T. J. Pinguet, O. Levi, L. A. Eyres, J. S. Harris, M. M. Fejer, B. Gerard, L. Becouarn, E. Lallier (presented at Conference on Lasers and Electro-Optics, Long Beach, CA, May 19-24, 2002).

"Widely tunable difference frequency generation in a multi-grating orientation-patterned GaAs," O. Levi, P. S. Kuo, X. Yu, J. S. Harris, M. M. Fejer, S. E. Bisson, T. J. Kulp, D. Bliss, and D. Weyburne, in Conference on Lasers and Electro-Optics/Quantum Electronics and Laser Science 2005 (Optical Society of America, Washington, DC, 2005), paper CWE5.

1d) Chalcopyrites for nonlinear optics – preparation, characterization, and defect modeling
West Virginia University (Giles/Halliburton)
Michigan Technological University (Pandey)
Stanford University (Feigelson)

"Luminescence associated with copper in ZnGeP_2 ," Lijun Wang, Lihua Bai, K. T. Stevens, N. Y. Garces, N. C. Giles, S. D. Setzler, P. G. Schunemann, and T. M. Pollak, *Journal of Applied Physics* **92**, 77-81 (2002).

"Electron paramagnetic resonance and electron-nuclear double resonance study of the neutral copper acceptor in ZnGeP_2 ," K. T. Stevens, L. E. Halliburton, S. D. Setzler, P. G. Schunemann, and T. M. Pollak, *Journal of Physics: Condensed Matter* **15**, 1625-1633 (2003).

"Optical and EPR study of defects in cadmium germanium arsenide," Lihua Bai, N. Y. Garces, Nanying Yang, P. G. Schunemann, S. D. Setzler, T. M. Pollak, L. E. Halliburton, and N. C. Giles, *Materials Research Society Proceedings* **Vol. 744**, 537-542 (2003).

"Infrared absorption bands related to native defects in ZnGeP_2 ," N. C. Giles, Lihua Bai, M. M. Chirila, N. Y. Garces, K. T. Stevens, P. G. Schunemann, S. D. Setzler, and T. M. Pollak, *Journal of Applied Physics* **93**, 8975-8981 (2003).

"Electron paramagnetic resonance of Cr^{2+} and Cr^{4+} ions in CdGeAs_2 crystals," N. Y. Garces, N. C. Giles, L. E. Halliburton, P. G. Schunemann, R. Feigelson, and K. Nagashio, *Journal of Applied Physics* **94**, 7567-7570 (2003).

"Correlation between dislocation etch pits and optical absorption in CdGeAs_2 ," K. Nagashio, A. Watcharapason, K. T. Zawilski, R. C. DeMattei, R. S. Feigelson, L. Bai, N. C. Giles, L. E. Halliburton, and P. G. Schunemann, *Journal of Crystal Growth* **269**, 195-206 (2004).

"A theoretical study of the group-IV antisite acceptor defects in CdGeAs_2 ," M. A. Blanco, A. Costales, V. Luana, and R. Pandey, *Applied Physics Letters* **85**, 4376 (2004).

"Luminescence and optical absorption study of p-type CdGeAs_2 ," Lihua Bai, J. A. Poston, Jr., P. G. Schunemann, K. Nagashio, R. S. Feigelson, and N. C. Giles, *Journal of Physics: Condensed Matter* **16**, 1279-1286 (2004).

"Donor-acceptor pair emission near 0.55 eV in CdGeAs_2 ," Lihua Bai, N. C. Giles, P. G. Schunemann, T. M. Pollak, K. Nagashio, and R. S. Feigelson, *Journal of Applied Physics* **95**, 4840-4844 (2004).

"Optical absorption and electron-nuclear double resonance study of Ni^{2+} ions in AgGaSe_2 crystals," K. T. Stevens, N. Y. Garces, Lihua Bai, N. C. Giles, L. E. Halliburton, S. D. Setzler, P. G. Schunemann, T. M. Pollak, R. K. Route, and R. S. Feigelson, *Journal of Physics: Condensed Matter* **16**, 2593-2607 (2004).

"Luminescence study of donors and acceptors in CdGeAs_2 ," Lihua Bai, P. G. Schunemann, T. M. Pollak, and N. C. Giles, *Optical Materials* **26**, 501-505 (2004).

"Assignment of infrared absorption bands in ZnGeP_2 ," N. C. Giles, Lihua Bai, N. Y. Garces, P. G. Schunemann, and T. M. Pollak, in SPIE Conference on Nonlinear Frequency Generation and Conversion: Materials, Devices, and Applications III, Proceedings Vol. 5337, 11-21 (2004).

"Effect of donors and acceptors on the optical properties of cadmium germanium arsenide (CdGeAs_2)," Lihua Bai, N. Y. Garces, L. E. Halliburton, N. C. Giles, P. G. Schunemann, K. Nagashio, and R. S. Feigelson, in SPIE Conference on Nonlinear Frequency Generation and Conversion: Materials, Devices, and Applications III, Proceedings Vol. 5337, 22-29 (2004).

"Optical Properties of CdGeAs_2 ," Lihua Bai, PhD dissertation, West Virginia University, 2004.

"Temperature dependence of polarized absorption bands in p-type CdGeAs_2 ," Lihua Bai, N. C. Giles, and P. G. Schunemann, Journal of Applied Physics 97, 023105/1-6 (2005).

"Urbach rule used to explain the variation of the absorption edge in CdGeAs_2 crystals," Lihua Bai, Chunchuan Xu, P. G. Schunemann, K. Nagashio, R. S. Feigelson, and N. C. Giles, Journal of Physics: Condensed Matter 17, 549-558 (2005).

"Electron-nuclear double resonance of Mn^{2+} ions in ZnGeP_2 crystals," N. Y. Garces, L. E. Halliburton, P. G. Schunemann, S. D. Setzler, and T. M. Pollak, Physical Review B 72, 033202/1-4 (2005).

"Optical absorption issues in CdGeAs_2 single crystals," K. Nagashio, Lihua Bai, R. DeMattei, N. C. Giles, and R. S. Feigelson, in SPIE Conference on Operational Characteristics and Crystal Growth of Nonlinear Optical Materials II, Proceedings Vol. 5912, 129-137 (2005).

"Photoluminescence of n-type CdGeAs_2 ," Lihua Bai, Chunchuan Xu, K. Nagashio, Chunhui Yang, R. S. Feigelson, P. G. Schunemann, and N. C. Giles, Journal of Physics: Condensed Matter 17, 5687-5696 (2005).

"Correlation of electrical and optical properties of CdGeAs_2 ," Lihua Bai, Chunchuan Xu, N. C. Giles, K. Nagashio, and R. S. Feigelson, Journal of Applied Physics 99, 013512/1-5 (2005).

"Effects of free carriers on the optical properties of n-type CdGeAs_2 :In," Lihua Bai, Chunchuan Xu, and N. C. Giles, Journal of Physics: Condensed Matter 18, 2741-2747 (2006).

"Improving optical transparency in CdGeAs_2 crystals by controlling crystalline defects," Robert S. Feigelson, Journal of Crystal Growth 292, 179-187 (2006).

"Electron paramagnetic resonance and electron-nuclear double resonance study of Mn^{2+} ions in CdGeAs_2 ," S. M. Evans, N. Y. Garces, R. C. DeMattei, R. S. Feigelson, N. C. Giles, and L. E. Halliburton, Physica Status Solidi B (appeared online Sept. 12, 2006).

Presentations:

"Optical properties of copper-doped ZnGeP_2 ," Lijun Wang, Lihua Bai, K. T. Stevens, N. C. Giles, S. D. Setzler, P. G. Schunemann, and T. M. Pollak; Poster presentation at the Thirteenth American Conf. on Crystal Growth and Epitaxy (ACCGE-13), Burlington, VT (Aug 12-16, 2001).

"Defect Issues in Ternary Chalcopyrites: Donors and Acceptors and Their Role in Optical Absorption", N. C. Giles, AFOSR Meeting of Contractors, 1 hour presentation, Stanford University, Stanford, CA (June 19, 2001).

"Optical and EPR Study of Defects in Cadmium Germanium Arsenide," Lihua Bai, N. Y. Garces, Nanyang Yang, P. G. Schunemann, S. D. Setzler, T. M. Pollak, L. E. Halliburton, and N. C. Giles; Poster presentation at the 2002 Fall Meeting of the Materials Research Society, Boston, MA (Dec 2-6, 2002).

"Identification and Characterization of Device-Limiting Point Defects in Chalcopyrites," Nancy C. Giles and Larry E. Halliburton, MURI Program Review for "Chalcopyrite and Orientation-Patterned Semiconductors for Mid-IR Sources: Modeling, Growth, and Characterization," 30 min presentation, Stanford University (Sept. 18, 2003).

"Crystal Growth and Etching Study of CdGeAs₂," Kosuke Nagashio, Anucha Watcharapasorn, Kevin Zawilski, Robert DeMattei, Robert Feigelson, Larry Halliburton, Nancy Giles, and Peter Schunemann, 15th American Conference on Crystal Growth and Epitaxy and 3rd International Symposium on Lasers and Nonlinear Optical Materials, Keystone, CO (July 21-23, 2003).

"Luminescence Study of Donors and Acceptors in Cadmium Germanium Arsenide," Lihua Bai, Nelson Garces, Larry Halliburton, Nancy Giles, Peter Schunemann, Scott Setzler, and Thomas Pollak, 15th American Conference on Crystal Growth and Epitaxy and 3rd International Symposium on Lasers and Nonlinear Optical Materials, Keystone, CO (July 21-23, 2003).

"EPR Investigation of Cr²⁺ and Cr⁴⁺ Ions in CdGeAs₂ Crystals," Nelson Garces, Lihua Bai, Nancy Giles, Larry Halliburton, Kosuke Nagashio, Robert Feigelson, and Peter Schunemann, 15th American Conference on Crystal Growth and Epitaxy and 3rd International Symposium on Lasers and Nonlinear Optical Materials, Keystone, CO (July 21-23, 2003).

"Optical Absorption, EPR, and Luminescence of Donors and Acceptors in Chalcopyrites: ZnGeP₂ and CdGeAs₂," Nancy C. Giles; Presentation at the Air Force Office of Scientific Research Semiconductor Materials Program Review, Williamsburg, VA (June 9-11, 2003).

"Effect of donors and acceptors on the optical properties of CdGeAs₂," Lihua Bai, N. Y. Garces, Chunchuan Xu, L. E. Halliburton, N. C. Giles, P. G. Schunemann, K. Nagashio, Chunhui Yang, and R. S. Feigelson, Photonics West 2004, San Jose, California (24-29 Jan 2004).

"Assignment of infrared absorption bands in ZnGeP₂," N. C. Giles, Lihua Bai, N. Y. Garces, T. M. Pollak, and P. G. Schunemann, Photonics West 2004, San Jose, California (24-29 Jan 2004).

"Absorption and Luminescence Studies of Nonlinear Optical Materials: CdGeAs₂ and ZnGeP₂," N. C. Giles and L. E. Halliburton, 2nd Symposium on Infrared Materials and Technologies, Pennsylvania State Univ. (State College, PA), Nov. 21-22, 2005.

1e) Fabrication and characterization of AlGaAs submicron waveguides and cavities **Stanford (Fejer/Harris)**

"Tightly confining AlGaAs waveguides and microcavities for optical frequency conversion," L. Scaccabarozzi, Z. Wang, X. Yu, W. T. Lau, M. F. Yanik, S. Fan, M. M. Fejer, J. S. Harris, Jr., Proc SPIE – Photonics West 2004, **5355**, pp. 111-119 (January 2004).

"Fabrication and characterization of tightly confining AlGaAs waveguides and microcavities for nonlinear optical applications," L. Scaccabarozzi, Z. Wang, X. Yu, M. M. Lee, W. T. Lau, M. F. Yanik, S. Fan, M. M. Fejer, J. S. Harris, Jr., Proc. SPIE--Photonics West 2005, **5728**, pp. 299-308 (January, 2005).

"Highly efficient birefringent second harmonic generation in submicron AlGaAs/Al_xO_y waveguides", L. Scaccabarozzi, X. Yu, S. Fan, M. M. Fejer, J. S. Harris Jr., Postdeadline session, Proc. OSA Conf. on Lasers and Electro-Optics (CLEO), Baltimore, MD (May 2005).

"Enhanced second harmonic generation in AlGaAs/Al_xO_y tightly confining waveguides and resonant cavities," Luigi Scaccabarozzi, Martin Fejer, Yijie Huo, Shanhui Fan, Xiaojun Yu, and James Harris, Opt. Lett., in press (2006).

"Artificially Birefringent Aluminum Gallium Arsenide/Aluminum Oxide-based Submicron Waveguides and Resonant Cavities for Nonlinear Optics," L. Scaccabarozzi, Ph. D. thesis, Stanford University, June 2006.

1f) Application of orientation-patterned GaAs for generation of terahertz radiation
Stanford (Fejer/Harris)

"Generation of multi-cycle THz-pulses via optical rectification in periodically inverted GaAs", Y-S Lee, K. L. Vodopyanov, W. C. Hurlbut, J. R. Danielson, V. G. Kozlov, D. F. Bliss, M. M. Fejer, Proceedings of SPIE **6120**, (2006).

"Optical generation of narrow-band terahertz packets in periodically-inverted electro-optic crystals: conversion efficiency, and optimal laser pulse format", K. L. Vodopyanov, Optics Express **6**, 2263 (2006).

"Optical generation of narrow-band terahertz packets in periodically-inverted electro-optic crystals: conversion efficiency, and optimal laser pulse format," Konstantin L. Vodopyanov, Optics Express **14**, 2263-2276 (2006).

Presentations

"Tunable 0.8-3.5 THz Source Based on Fiber-laser Pumped Orientation-patterned GaAs," Konstantin Vodopyanov, Joe Schaar, Martin Fejer, Xiaojun Yu, James Harris, Gennady Imeshev, Martin Fermann, David Bliss, David Weyburne, in Conference on Lasers and Electro-Optics/Quantum Electronics and Laser Science 2006 (Optical Society of America, Washington, DC, 2006), paper CtuGG5.

"Terahertz-Wave Generation in Periodically-Inverted GaAs," Konstantin L. Vodopyanov, M. M. Fejer, D. M. Simanovskii, V. G. Kozlov, Y. S. Lee, in Conference on Lasers and Electro-Optics/Quantum Electronics and Laser Science 2005 (Optical Society of America, Washington, DC, 2005), paper CWM1.

2) Experiments involving magnetic chalcopyrite and other semiconductors for potential Spintronic applications

Northwestern (Ketterson)

Mn-doped ZnGeAs₂ and ZnSnAs₂ single crystals: Growth and electrical and magnetic properties, S. Y. Choi, J. Y. Choi, S. C. Hong, S. L. Cho, Y. Kim, J. B. Ketterson, Journal of the Korean Phys. Soc. **42** S739- Suppl. S (2003).

Ferromagnetic properties in Cr, Fe-doped Ge single crystals, S. Choi, S. C. Hong, S. L. Cho, Y. Kim, J. B. Ketterson, C. U. Jung, K. Rhie, B. J. Kim, Y. C. Kim, J. Appld. Phys. **93** 7670 (2003).

Synthesis of new pure ferromagnetic semiconductors: MnGeP₂ and MnGeAs₂, S. Cho, S. Choi, G. B. Cha, S. C. Hong, Y. Kim, A. J. Freeman, J. B. Ketterson, Y. Park, and H. M. Park, Solid State Communications **129**: 609 (2004).

Magnetic anisotropy and transport properties of epitaxially grown MnAs/GaAs digital alloys, J. H. Song, Y. Cui, J. J. Lee, Y. Kim, J. B. Ketterson, S. G. Cho, Journal of Applied Physics **95** 7288-7290 Part 2, (2004).

Electronic and magnetic properties of MnSnAs₂, S. G. Cho, S. Y. Choi, G. B. Cha, S. C. Hong, Y. Park, H. M. Park, Y. Kim, J. B. Ketterson, Physica Status Solidi B-Basic Research **241**, 1462-1465 (2004).

Magnetic properties of MnGeAsP films grown on GaAs(100) by molecular beam epitaxy, Y. Cui, J. J. Lee, J. H. Song, L. Luan, Y. Kim, J. B. Ketterson, and S. Cho, Journal of Applied Physics **95**, 6515, Part 2 (2004).

Ferromagnetic properties of MnAs/Ge multilayers grown by molecular beam epitaxy, J. Lee, Y. J. Cui, J. H. Song, Y. K. Kim, A. J. Freeman, J. B. Ketterson, S. Cho, Journal of Applied Physics **95**, 6562 Part 2 (2004).

Control of the magnetic anisotropy of epitaxially grown MnAs/GaAs ferromagnet-semiconductor hybrid superlattices, J. H. Song, J. J. Lee, Y-j Cui, J. B. Ketterson and S. Cho, Applied Physics Letters **85**, 4079 (2004).

Ferromagnetism and coupling between charge carriers and magnetization at room temperature in Ge/MnAs multilayers, J. J. Lee, Y. Cui, J. H. Song, A. J. Freeman, J. B. Ketterson and S. L. Cho, Applied Physics Letters **85**, 3169 (2004).

Electrical-transport, magneto-transport and magnetic anisotropy of epitaxially grown MnAs/GaAs hybrid multilayers, J. H. Song, J. J. Lee, Y. Cui, J. B. Ketterson, S. L. Cho, J. Mag. Mater. **286** 41 (2005).

Room temperature ferromagnetism of Ge/MnAs digital alloys, J. J. Lee, M. Y. Kim, Y. Cui, J. H. Song, A. J. Freeman, and J. B. Ketterson, J. Superconductivity **18**, 75 (2005).

Growth-temperature dependence of magnetic and magneto-transport properties of epitaxially grown MnAs/GaAs hybrid multilayers, J. H. Song, J. J. Lee, Y. Cui, J. B. Ketterson, and S. Cho, J. Superconductivity **18** 105 (2005).

Room-temperature ferromagnetism in Cu-doped ZnO thin films, D. B. Buchholz, R. P. H. Chang, J. H. Song, and J. B. Ketterson, Appld. Phys. Lett. **87**, 082504 (2005).

Beta-phase-domain-free alpha-MnAs thin films on GaAs(001) by post-growth annealing, J. H. Song, Y. Cui, J. J. Lee, and J. B. Ketterson, Applied Physics Letters **87**, 092504 (2005).

Ferromagnetism of Mn/Ge, multilayers grown by molecular beam epitaxially, J. J. Lee, J. E. Medvedeva, J. H. Song, Y-j Cui, A. J. Freeman, and J. B. Ketterson, J. Superconductivity **18** 335 (2005).

Magnetic and transport properties of MnGeP₂ films grown on GaAs(001) by molecular beam epitaxy, Y-j Cui, W. Mu, J-j. Lee, J. Song, Y. Kim, Y. J. B. Ketterson, S. Cho, J. Applied Physics **97**, 10M518 Part 3 (2005).

Postgrowth annealing effects on heteroepitaxial MnAs thin films grown on GaAs(001) and Si(001) J. H. Song, Y. Cui, J. J. Lee, M. Y. Kim, and J. B. Ketterson, Journal of Applied Physics **99** (8): Art. No. 08D513 (2006).

X-ray absorption spectroscopy study of copper-doped zinc oxide: a high T_c diluted magnetic semiconductor, Q. Ma, L.-H. Ye, D.B. Buchholz, J.-H. Song, A.J. Freeman, J. B. Ketterson, R.P.H. Chang, SRMS5- 231 (2006).

Papers Submitted

Magnetic Properties of Ge/MnAs Digital Heterostructure, J. J. Lee, M. Y. Kim, J. H. Song, Y. Cui, A. J. Freeman, and J. B. Ketterson (TMAG-06-10-1539)

Papers in Preparation

Room temperature ferromagnetism in n-type Ge/MnAs digital alloys, J. J. Lee, M.Y. Kim, J. H. Song, Y. Cui, A. J. Freeman, and J. B. Ketterson

Ferromagnetic nanomultilayers for silicon-based room temperature spintronics, J. J. Lee¹, M. Y. Kim, J. H. Song, Y. Cui, A. J. Freeman, and J. B. Ketterson.